Absorption in Gamma Ray Burst afterglows

G. Stratta[1], F. Fiore and L. A. Antonelli

Osservatorio Astronomico di Roma, Via Frascati 33, I-00044 Monteporzio Catone, Italy

and

L. Piro and M. De Pasquale[1]

Istituto di Astrofisica Spaziale & Fisica Cosmica, C.N.R., Via Fosso del Cavaliere 100, I-00133, Roma, Italy

ABSTRACT

We studied the X-ray and optical absorption properties of 13 Gamma Ray Burst afterglows observed by BeppoSAX. We found that X-ray absorption in addition to the Galactic one along the line of sight is highly statistically significant in the two cases with the best statistics (probability $> 99.9\%$). In three other cases the presence of X-ray absorption is marginally significant (probability $\sim 97\%$). Measured rest frame absorbing column densities of hydrogen, N_H, range from 0.1 to 10.0 $\times 10^{22}$ cm^{-2} (at 90% confidence level) assuming a solar metal abundance. X-ray absorption may be common, although the quality of present data does not allow us to reach a firm conclusion. We found that the rest frame column densities derived from XMM and Chrandra data as quoted in the literature are in good agreement with the BeppoSAX estimated rest frame N_H range, supporting our result. For the same GRB afterglow sample we evaluated the rest frame visual extinction A_{Vr}. We fitted the optical-NIR afterglow photometry with a power law model corrected at short wavelengths by four different extinction curves. By comparing X-ray absorptions and optical extinction, we found that if a Galactic-like dust grain size distribution is assumed, a dust to gas ratio lower than the one observed in the Galaxy is required by the data. A dust to gas ratio $\sim 1/10$ than the Galactic one, as in the Small Magellanic Cloud (SMC) environment, has been tested using the SMC extinction curve, which produces good agreement between the best fit N_H and A_{Vr}. We note, however, that the best fit N_H values have been obtained by assuming solar metal abundances, while the metallicity of the SMC ISM is $\sim 1/8$ the solar one (Pei 1992). If such

[1]Dipt. di Fisica, Universita' "La Sapienza", P.le A. Moro 5, I-00187 Roma, Italy

low metallicity were assumed, the best fit N_H values would be higher by a factor of ~ 7, providing a significant increase of the χ^2. Alternative scenarios to explain simultaneously the optical and X-ray data involve dust with grain size distributions biased toward large grains. Possible mechanisms that can bring to such a grain size distribution are discussed.

Subject headings: gamma rays: bursts — dust, extinction — X-rays: general

1. Introduction

Soon after the γ-ray flash, optical and X-ray afterglows of Gamma Ray Bursts (GRB) are among the brightest sources in the sky at cosmological redshifts. More than thirty GRB redshifts have been measured to date and their distribution ranges from 0.168 (Greiner et al. 2003) to 4.5 (Andersen et al. 2000) with a median of z $\sim$ 1.1 (excluding GRB 980425 if at z=0.0085). Follow-up observations of the GRB localized by BeppoSAX, the IPN and by the RXTE and HETE2 satellites, show that tens of minutes after the GRB the optical afterglow can be as bright as R=14-16 mag; a few hours later it can still be as bright as R=17-19 mag. An exceptionally bright example is the case of GRB 030329 for which the optical afterglow reached R=12.7 mag at 1.5 hours from the GRB and it decreased down to R=19 mag after $\sim$ 10 days (e.g. Price et al. 2003; Stanek et al. 2003). The X-rays afterglow can be as bright as the Crab Nebula a few minutes after the GRB, while 5-8 hours later it can be as bright as a bright AGN, i.e. $\approx$mCrabs (see Frontera et al. 2000, also Fiore et al. 2000 for an estimate of the GRB afterglows logN-logF in the range 0.5-2.0 keV, where fluxes are integrated from minutes up to hours after the GRB event). This opens up the perspective for gathering spectra of high quality of sources at cosmological redshifts, provided that the afterglow can be observed in such short time scales. Spectral studies of GRB afterglows can provide crucial data on the environments in which GRB occurs. This can give us both important constraints on the nature of the GRB progenitor and on the interstellar matter (ISM) in the GRB host galaxies.

Candidate GRB progenitor include: 'collapsars' (Woosley 1993, Paczynski 1998; MacFadyen & Woosley 1999), 'supranovae' (Vietri & Stella 1998), mergers of two neutron stars or a neutron star and a black hole (e.g. Eichler et al. 1989; Paczynski 1990; Narayan, Paczynski & Piran 1992; Meszaros & Rees 1992).

Multiwavelength afterglow observations suggest the association of "long GRB" (for which the duration of the prompt event peaks at $\sim$ 20s, e.g. Norris, Scargle & Bonnell 2000) progenitor with massive stars. Some indications are, among others: i) the GRB loca-

tions relative to their host galaxy (Bloom, Kulkarni & Djorgovski 2002a); ii) the detection of iron lines in the X-ray afterglow spectrum of five GRB (Piro et al. 1999, 2000; Yoshida et al. 1999; Antonelli et al. 2000; Amati et al. 2000); iii) the presence of late re-brightening in the light curves of some afterglows, interpreted as the evidence of an underlying supernova (e.g. Bloom et al. 2002b); iv) the presence of supernova features emerging in the optical afterglow spectra of GRB 030329 (Stanek et al. 2003, Hjorth et al. 2003; Kawabata et al. 2003) and of GRB 021211 (Della Valle et al. 2003). Because of the short lifetimes of massive stars, it is likely that their collapse happens close to their star forming region, that is, close to a dense and dusty environment (e.g. Fryer, Woosley & Hartman 1999; Perna & Belczynski 2002a). Therefore, one important element in favor of massive star progenitor would be the evidence of strong dust extinction. Indeed, the non detection of the $\sim 60\%$ of X-ray afterglows at optical wavelengths (dark GRB), favors this hypothesis. However, the optical spectra of GRB afterglows, do not generally show strong reddening (Simon et al. 2001; Galama & Wijers 2001). Moreover, Lazzati, Covino & Ghisellini (2002) show that even if dark GRB are located in the innermost regions of Galactic-like molecular clouds, in several cases the corresponding visual extinction is not enough to hide their optical afterglows. Therefore, a more accurate study of the GRB environment is needed.

Prompt observations of GRB afterglows offer a new and distinctive path for the study of the matter in the immediate surroundings of the GRB, r$\sim$1-10 pc (Perna & Loeb 1998; Böttcher et al. 1999; Perna et al. 2002b; Perna & Lazzati 2002c; Fox et al. 2003) and in the GRB host galaxy (Ciardi & Loeb 2000; Fiore 2001; Bloom et al. 2002a; Savaglio, Fall & Fiore 2003) X-ray and optical-UV spectroscopy can tell us about gas density and ionization status, metal abundances, dust content and kinematics of the matter in the GRB environment. This can be done by using both emission features and absorption features (see e.g. Kumar & Narayan 2003; Böttcher et al. 1999; Piro et al. 2000; Ghisellini et al. 2002). Although absorption features are more difficult to study than emission lines, they carry with them unbeatable information, because they probe matter along a single beam, i.e. along the line of sight to the background beacon. This greatly reduces the complications related to the matter geometry and dynamics, which strongly affects emission line studies. Even when such emission or absorption features are not detected or are not resolved, X-ray spectra can provide useful information from measures of low energy cut-offs due to photoelectric absorption

Moreover, GRB afterglows can be used to study the ISM of their host galaxies. High redshifts galaxies have so far been studied mainly via 'Lyman-break galaxies' (e.g. Steidel et al. 1999), and via galaxies which happen to lie along the line of sight to bright quasars, notably the 'Damped Lyman-alpha' systems (DLA, e.g. Pettini et al. 1997, 1999). However, probably neither of these methods gives an undistorted view of the bulk of the typical

high redshifts galaxy. Lyman-break galaxies are characterized by pronounced star-formation and their inferred chemical abundances may be related to these regions rather than being representative of typical high z galaxies (see e.g. Steidel et al. 1999). DLA studies are likely to be biased against dusty systems, since these would hide the background quasars in color-based surveys. Furthermore, DLA are often identified with dwarf or Low Surface Brightness galaxies and therefore may not be representative of the full high z galaxy population. On the other hand, GRB seem to occur well within the main body of their host galaxies, not in the outer halos (Bloom et al. 2002a), therefore, GRB afterglows can provide a powerful, independent tool to study the ISM of high redshifts galaxies (Castro et al. 2003, Mirabal et al. 2002, Fiore 2001; Savaglio et al. 2003). The latter authors compared metal column density in GRB host galaxies with those of DLAs. They find that while the column densities of iron and magnesium are similar or slightly higher than that in DLAs, the column of zinc are significantly higher. Since iron and magnesium, unlike zinc, tend to be depleted in dust, this finding indicates that a significant fraction of these elements is in dust since not observed through absorption lines, thus GRB are probably probing denser and dustier regions, than DLAs.

We present in this paper the results of a systematic spectral analysis of 13 GRB afterglows observed by BeppoSAX in X-rays, and by several ground based telescopes in optical-UV, aimed at measuring and constraining the X-ray absorption along the line of sight as well as the extinction in the optical-UV bands. The comparison of the results obtained in the two spectral band will provide constraints on the dust to gas ratio of the absorbing matter and on the dust properties, as seen from several hours to a few days from the GRB event.

The paper is organized as follows: §2 shows the BeppoSAX X-ray afterglow selected sample; §3 presents the X-ray data reduction and spectra extraction procedures, along with a discussion on the systematics affecting the column density measurements; §4 presents the optical photometry of 9 GRB afterglows of our sample with a detected optical counterpart; results are presented and discussed in §5 and §6 respectively.

2. The BeppoSAX X-ray bright afterglow sample

We selected from the BeppoSAX archive all the X-ray afterglows observed during a period of four years (from February 1997 to February 2001) that have enough counts in the Medium Energy Concentrator Spectrometer (MECS) to extract a spectrum and to perform a spectral analysis, that is, with a signal to noise ratio $S/N \gtrsim 7$ in the 2.0-10.0 keV. We also required that the Low Energy Concentrator Spectrometer (LECS) 0.1-2 keV spectra contain at least 20 counts, or that the counts expected in this LECS band, based on simulations

performed using the best fit power law model obtained from the MECS spectrum and assuming a column density equal to the Galactic value along the line of sight, are also smaller than the above threshold at the 2σ confidence level, not to miss bright and highly obscured afterglows. The number of afterglow observations satisfying these requirements is 13.

Table 1 summarize the selected GRB X-ray afterglows along with the Galactic hydrogen column density along the line of sight to each GRB, as determined from the coarse, ~ 3 deg resolution, maps of Dickey & Lockmann (1990), the host galaxy redshifts if known, the R.A. and Dec. coordinates and the optical detection. Redshifts measurements are from optical spectroscopy except for GRB 000214 (Antonelli et al. 2000), for which a redshifts of 0.47 ± 0.06 was inferred assuming that the observed emission line is the iron K_α line at 6.7 keV (rest frame).

3. BeppoSAX data reduction and analysis

The GRB afterglows observations were performed with the BeppoSAX Narrow Field Instruments (NFI), LECS 0.1-10 keV (Parmar et al. 1997), MECS 1.3-10 keV (Boella et al. 1997), HPGSPC 4-60 keV (Manzo et al. 1997) and PDS 13-200 keV (Frontera et al. 1997). LECS (1 unit) and MECS (3 units) are imaging gas scintillation proportional counters, the HPGSPC is a collimated High Pressure Gas Scintillation Proportional Counter and the PDS consists of four collimated phoswich units. We report here the analysis of only the LECS and MECS data because GRB afterglows are usually many times fainter than the PDS and HPGSPC internal backgrounds.

After 1997 May 6^{th} MECS observations were performed with MECS2 and MECS3 units only because on this date a technical failure caused the switch off of the MECS1 unit. For all the selected GRB sample, data from the MECS2 and MECS3 units were combined together, after gain equalization, to increase the signal to noise ratio. In the case of GRB 970228 (that is the only GRB in our sample observed before 1997 May) we used the data from MECS3 only, since the source happened to lie just below the Beryllium strongback support of the MECS1 and MECS2 windows (which basically absorbs all photons below about 5 keV).

Standard data reduction was performed using the SAXDAS software package version 2.0 following Fiore, Guainazzi & Grandi (1999).

LECS and MECS spectra were extracted from regions of radii between 3 and 8 arcmin, chosen to maximize the count rate in the 0.5-2 keV and 2-10 keV band respectively. The choice of the extraction radius depends on the source and background intensity, and on the instrument Point Spread Function, PSF. The 90% encircled energy generally is within 3-4

arcmin for the MECS and within 6-8 arcmin for the LECS (Fiore et al. 1999).

Background spectra were extracted in detector coordinates from high Galactic latitude ($|b| > 20$ deg) "blank fields" (averaged LECS and MECS pointing of sky regions without strong X-ray sources, for a total exposure of about half a million of seconds in both instruments, Fiore et al. 1999) using the same source extraction regions. "Local" background cannot be safely used when analyzing LECS and MECS spectra, because of the relatively broad PSF and because the background strongly varies with the position in the detector (Fiore et al. 1999 and Chiappetti et al. 1998). We have compared the mean level of the background in the LECS and MECS "blank fields" observations to the mean level of the background in the GRB observations using source free regions at various positions in the detectors. The "local" MECS background count rate is within 2% than that in the "blank fields". On the other hand, the "local" LECS background count rate differs from that of the "blank fields" by up to 20% in 7 cases. In these cases the "blank fields" background spectrum was multiplied by appropriate correction factors before subtraction from the source spectrum.

Usually, the position of GRB afterglows is not know with accuracies better than several arcminutes at the moment of the BeppoSAX NFI pointing. On these scales the vignetting of the telescopes varies significantly (see e.g. Fiore et al. 1999). Furthermore, the LECS thin polypropylene window is supported by a mesh of grids of tungsten wires that introduces a complicated pattern of obscuration. The actual value of obscuration strongly depends on the exact position of the source centroid in detector coordinates. The spacing of the thicker wire grid is of about 2 arcmin, much less than the uncertainty on the afterglow position. This means that the afterglow position in detector coordinates with respect to the thick wire grid cannot be known 'a priori' as well as the level of the grid obscuration. For these two reasons we therefore not used the standard on axis effective area files, but we evaluated the instrument effective area at the afterglow position in detector coordinates (we used the SAX/LECS data analysis software LEMAT). These 'ad hoc' effective area file takes correctly into account the energy dependent telescope vignetting and the photons absorbed by the LECS support mesh wires. On axis redistribution matrices, from the December 1999 release have been used for both LECS and MECS, since these depend very little on the source position in the detectors.

Table 2 gives the LECS and MECS exposure times, optimum extraction radius, background and source count rates. Note that LECS exposure times are usually smaller than MECS ones since it is operated during dark time only.

Table 3 gives the MECS off-axis angles, the time interval between the GRB trigger and the NFI pointing, the LECS 'raw' detector pixel coordinates of the source, at which the

effective area has been computed.

To get Gaussian statistics and so to ensure the applicability of the χ^2 test to evaluate the goodness of our fits, LECS and MECS spectra were rebinned to obtain at least 20 counts per energy channel. We then performed simultaneous LECS and MECS spectral fitting using the bands 0.1(or 0.4 keV, see below) 4.0 keV and 1.6-10.0 keV in the two instruments respectively (see §5.1). Errors quoted in this paper for the column density and the spectral index are 90% confidence intervals for two parameters of interest ($\Delta\chi^2 = 4.61$), unless differently specified.

3.1. Systematic errors on Column Density estimates

3.1.1. Galactic Column Densities

The knowledge of the Galactic column density along the line of sight to each burst is crucial for our study. Relatively small errors in the evaluation of the Galactic columns would translate in a larger errors on the rest frame absorption, since best fit N_H values scale with redshift as $(1+z)^{\sim 2.6}$ (the photoelectric cross section scaling with energy roughly as $E^{-2.6}$). The values in Table 1 have been obtained interpolating on a grid with spacing of 3 degrees (Dickey & Lockmann 1990). It is well known that the Galactic column density can vary on much smaller scales (Elvis, Lockman & Wilkes 1989). To evaluate the average magnitude of this variation we compared the Galactic column density obtained using the coarse 3 degrees 21 cm emission maps along the line of sights of a sample of AGN for which an accurate 21 cm emission measurements were already performed by using a 21 arcmin beam NRAO 140 ft telescope at Green Bank by Elvis et al. (1989). We found that the average ratio between the two determinations is close to 1 and that the standard deviation is of 0.16, independent of the value of the Galactic column density. The highest positive deviation found is of 50%. We therefore performed for each GRB three series of fits, one with the nominal Galactic N_H value and the other two by increasing this value by 16% and 50% respectively, to check whether additional extra galactic absorption would still be significantly even in case the Galactic column has been underestimated in the Dickey & Lockmann (1990) maps.

Another tracer of the column density of matter in a given direction is the infrared emission at 100μm. This can therefore be used as a further check of the Galactic column density values given in Table 2. We used the IRAS faint source survey to search for any "cirrus" contamination along the line of sight of each GRB. We used a 10 to 30 arcmin radius search region to measure the 100μm MJy/sr brightness S_{100}. By adopting $dS_{100}/dN_H = 0.5 - 2.0$ MJy/sr 10^{20} cm^{-2} as typical Galactic dust to gas ratio (Reach, Heiles & Koo 1993; Heiles, Reach & Kooh 1988; de Vries, Heithausen & Thaddeus 1987) we estimated

the implied N_{HGal} values and then compared them with the maps of Dickey & Lockmann (1990). All the inferred N_{HGal} values reveal no absorption excess due to presence of cirrus along the analyzed line of sight.

3.1.2. Background subtraction

The background subtraction procedure previously described works well if the Galactic column density along the line of sight to the GRB, is not much higher (or lower) than that in the "blank fields". Otherwise the background low energy spectrum (e.g. below 0.3 keV) would be very different from that of the "blank fields". Blank fields are all at high Galactic latitude, and the average Galactic column density along their line of sight is $\sim 3 \times 10^{20}$ cm^{-2}. Several afterglows in our sample have a Galactic column density much higher than this value (see Table 2). Adopting the "blank field" background spectrum for those afterglows at Galactic $N_H \gtrsim 5 \times 10^{20}$cm^{-2} it would results in an over-subtraction of the background below 0.3-0.4 keV and in a consequent overestimate of the intrinsic absorbing column. As an example, the 0.2 keV flux would decrease by $\sim 90\%$ by increasing N_H from 3×10^{20}cm^{-2} to 5×10^{20}cm^{-2}. At 0.4-0.5 keV the flux would decrease by much smaller amount, of the order of 10-20%. We therefore decided to limit the spectral analysis of the afterglows with Galactic column densities higher than 5×10^{20} cm^{-2} to energies higher than 0.4 keV.

3.1.3. LECS-MECS calibration of the normalization factor

A Constant normalization factor must be introduced in the fitting models in order to take into account the systematic error in the knowledge of the absolute LECS and MECS normalization factor (Fiore et al. 1999). Assuming the MECS as reference instrument, the expected factor between LECS and MECS for constant sources is about 0.9 ± 0.2. However, GRB afterglows are not constant sources: their flux decreases usually as a power law with index δ in the range $-1 \div -1.5$ (see e.g. Costa et al. 1999; Piro 2002a). Moreover, the non completely simultaneous observations of the LECS and MECS instruments due to the switch-off of the LECS during part of the orbit, introduces a further complication in the determination of the normalization factor. We have therefore decided to leave completely free the normalization factor in the fits.

We are aware that letting the normalization factor be free to vary introduces an additional degree of freedom in the fit and consequently increases the uncertainty on the derived N_H. In fact, a truly curved spectral shape toward the lower energies could be mimicked, in

spectra of low statistics, by a lower MECS to LECS normalization factor. As an example a factor of ~ 2 lower normalization factor, could mimic a factor of $\sim 3-4$ lower N_H. The 68% LECS-MECS normalization factor confidence intervals are reported in Tables 5 and 6.

4. Optical data

For 9 of the 13 selected GRB with X-ray afterglow an optical afterglow was also discovered (see Table 1). We collected the optical and near infrared magnitudes of these nine GRB from the literature to study the extinction properties through the comparison of dust extinction models to the afterglow Spectral Energy Distribution (SED).

We selected, among the large number of papers reporting photometric data on a given GRB optical afterglow, those works containing the widest possible frequency coverage and the best and most complete documentation. We list and discuss the references used for each GRB afterglow in the appendix section.

Observations in different bands are usually performed at different times. Since optical afterglows are sources with fluxes rapidly decaying in time, their magnitudes have been extrapolated to a single specific time t_0. The t_0 was selected to be as close as possible to the first optical observations, to keep the statistical uncertainties on the observed magnitudes small. The extrapolation of the observations at different bands at t_0 was performed by adopting the best fit decay index quoted in the literature.

Corrections for the Galactic interstellar extinction have been performed, unless explicitly specified, using the IRAS 100 μm E(B-V) maps by Schlegel, Finkbeiner & Davis (1998, SFD) and we derived the extinction at different wavelengths using the extinction curve parameterization by Cardelli, Clayton & Mathis (1989) assuming $R_V = A_V/E(B-V) = 3.1$.

Table 4 gives for each GRB the magnitude in each photometric bands, extrapolated at t_0 (see notes on Table 4) and corrected for Galactic extinction. We conservatively kept the error on the magnitudes to 0.03 mags when the published error is smaller that this value.

GRB 000926 is not part of our BeppoSAX sample because its X-ray data has poor statistics (see section 2). However, it has relatively high quality Chandra data and a complete optical-NIR photometry. Furthermore, GRB 000926 has been observed at a medium-high resolution with Keck ESI (Castro et al. 2003) and Savaglio et al. (2003) were able to derive information on the metal column densities from this spectrum. For these reasons, we decided to include it in our analysis. We take the photometry of GRB 000926 (U, B, V, R, I, J, H and K) from Fynbo et al. (2001) and the Galactic extinction in the direction of this burst

from the SFD maps as $A_V = 0.07$. The redshift of GRB 000926 is $z = 2.0379 \pm 0.0008$ (Castro et al. 2003).

The optical to near infrared SEDs of the nine GRB afterglows are shown in Figure 1.

5. Results

In this section we summarize the results of afterglow spectral fitting, performed separately in the X-ray and in the optical-NIR energy ranges. Our goal is to estimate the absorption in the soft X-ray energy and extinction in the optical band.

5.1. X-ray spectral fittings

At the time of the NFI observations (on average after ~ 10 hours after the GRB event, see Table 3), afterglow X-ray spectra are usually well described by simple power laws. We therefore performed a spectral fit by adopting a simple power law model with two photoelectric absorption component: one representing the absorption from our Galaxy and the other representing the additional absorption along the line of sight.

The quality of the data does not allow to fit for the absorber redshift. We therefore present in Table 5 (0.1-10 keV band) and Table 6 (0.4-10 keV band) best fit parameters obtained with the additional absorber at the redshift of the GRB, or at z=1 when the redshift of the GRB is unknown, since GRB redshift distribution peaks at about this value (Djorgovski et al. 2001).

Tables 5 and 6 also give the results of the fits performed fixing the redshift of the additional absorbing column to zero. Figure 2 shows the best fit additional column density at z=0 against the Galactic column. No trend is evident, supporting the robustness of our analysis.

Figure 3 shows the best fit additional absorbing column density measured at z=0 and at z=z_{GRB} (or z=1 for the GRB with unknown redshift) as a function of the redshift. Since the photoelectric cross section scales with energy roughly as $E^{-2.6}$, effective N_H values scale with redshift as $(1+z)^{2.6}$. Consequently, fitting the absorption in the GRB frame the resulting column is highly magnified with respect to that fitted at z=0 and small errors in the evaluation of the Galactic column would translate in a strong trend of the additional column with z toward high N_H values at high z. This is not observed, supporting the robustness of our analysis.

To evaluate the statistical significance of a given additional N_H measurement we used the F test (Bevington & Robinson 1992). We found that in two cases, GRB 990123 and GRB 010222, the improvement of the χ^2 including the additional absorber to the fit is highly significant (Figure 4), probability $> 99.99\%$. In both cases the probability remains higher than 99.99% increasing $N_{HGal.}$ by 16% (that correspond to 68 % of uncertainty on our estimate of the Galactic column along the line of sight, see §3.1.1). Even increasing $N_{HGal.}$ by 50% (the highest deviation we expect from our estimates of $N_{HGal.}$) the probability remains higher than 99.99% for GRB 010222 and higher than 98 % for GRB 990123.

In three other cases (GRB 980703, GRB 990510 and GRB 001109) the improvement of the χ^2 including the additional absorber to the fit is marginally significant (probability of 97%). In all these cases increasing $N_{HGal.}$ by 16% reduces the statistical significance of the χ^2 improvement below the threshold of 95%.

We conclude that the detection of absorption in addition to the Galactic one is robust against statistical and systematic uncertainties in 2 of the 13 GRB analyzed (GRB 990123 and GRB 010222). We note that the spectra of GRB 990123 and GRB 010222 are also those with the best statistics. However, fitting the spectra of two other GRB afterglows with lower but still reasonably good statistics, GRB 971214 and GRB 970228, including an additional absorber, does not produce a significant improvement in χ^2 (probability of 93.3% and 90.8% respectively). For the rest of the sample, additional absorption may be common, although the quality of the data in the majority of the cases does not allow highly significant detection.

Assuming that the most of the matter responsible of absorption is at the GRB redshift, we found N_H rest frame values in the range $0.1 - 10.0 \times 10^{22}$ cm^{-2} (90% confidence level), similar to the column usually observed toward the disk and the bulge of our Galaxy (see Figure 3).

5.1.1. GRB 010222

A more detailed analysis has been performed for this burst which is the second brightest X-ray afterglow of the selected sample and shows a peculiar behavior at low energies (Figure 4).

We note from Table 5 that our N_H measurement for this burst, is somehow lower, but still consistent with the N_H reported by in't Zand et al. (2001) ($N_H = 2.5 \times 10^{22}$ cm^{-2}) using the same BeppoSAX data (0.3-10.0 keV). On the other hand, our measure is higher than that one reported by Björnsson et al. (2002) $N_H = (6.5 \pm 0.11) \times 10^{21}$cm^{-2}, using

Chandra observations (0.5-10.0 keV). We note, however, that the Chandra data are affected by pile-up. This introduces an additional systematic uncertainty in the spectral parameter estimates.

The low energy absorption for this burst, may show possible complexities and/or variability. In fact, the presence of a neutral absorber produces a good fit at energies $\gtrsim 0.5$ keV but at lower energies an excess with respect to the best fit model is observed (Figure 5). There are at least two possible explanations for these residuals: 1) the recovery of the spectrum below the energies of strong absorption edges of OVII (0.74/(1+z)=0.30 keV), OVIII (0.87/(1+z)=0.35 keV); 2) the spilling of the emission spectrum through a leaky absorber. We tested both models. First we fitted to the data a ionized absorber model ('absori' in XSPEC) at the redshift of the host galaxy. We obtained a good fit ($\chi^2 = 92.0$ with 110 degrees of freedom, d.o.f.) with a rest frame column density of $1.8^{+1.2}_{-0.9} \times 10^{22}$ cm^{-2} and a ionization parameter of $\xi = 7.6^{+17.4}_{-7.1}$ (Figure 5). The probability for a chance improvement in χ^2 is 0.3% using the F-test. Second, we fitted a partial covering absorber ('zpcfabs' in XSPEC). In this case we obtain a similarly good fit ($\chi^2 = 92.5$ with 110 d.o.f.), a rest frame column density of $1.9^{+1.3}_{-0.9} \times 10^{22}$ cm^{-2} and a cover fraction of 0.8 ± 0.1. The probability for a chance improvement in χ^2 is 0.4% using the F-test.

To check for the presence of a narrow iron K_α emission line we added to the simple power law model a Gaussian component, fixing its width to $\sigma = 0.01$ keV and letting its energy to be free to vary in the range 6.4-6.9 keV rest frame. We found an upper limit to the line intensity of $I = 1.7 \pm 10^{-5}$ photons s^{-1} cm^{-2} (90% confidence level) and an upper limit to its equivalent width (EW) of 0.15 keV.

5.1.2. Additional X-ray observations

We compared our BeppoSAX results with other rest frame column density measures that became available, thanks to Chandra and XMM data for 9 additional GRB at known redshift.

Ballantyne et al. (2002) found a 90% upper limit of $N_H = 0.64 \times 10^{22}$ cm^{-2} at z=1.0 for GRB 991216 using 0.4-8.0 keV Chandra data.

Piro et al. (2001) and (2002b), estimated for GRB 000926 and for GRB 000210, $N_H = 4.0^{+3.5}_{-2.5} \times 10^{21}$ cm^{-2} at z=2.04 and $N_H = (5 \pm 1) \times 10^{21}$ cm^{-2} at z=0.846 respectively, using Chandra *and* BeppoSAX data. Note here that Harrison et al. (2001) do not present evidences for significant absorption in addition to the Galactic one for GRB 000926 at the redshift of the host galaxy using Chandra data.

Reeves et al. (2002) and Borozdin & Trudolyubov (2003) do not detected any significant absorption above the Galactic value in the X-ray spectra of GRB 011211 using XMM data.

Watson et al. (2002) measured a rest frame $N_H = (1.3 \pm 0.2) \times 10^{22}\mathrm{cm}^{-2}$ at $z = 1.8$ for GRB 020322 using XMM. However, the uncertainty on the redshift estimated directly from the X-ray data ($z = 1.8^{+1.0}_{-1.1}$) is large. The confidence interval plotted for this burst in Figure 3 includes the uncertainty over z in addition to the statistical uncertainty.

Mirabal et al. (2002b) measured $N_H = (4.7 \pm 3.7) \times 10^{21}$ cm^{-2} for GRB 020405 at z=0.690, using Chandra data.

Butler et al. (2003) found no additional absorption for the X-ray afterglow spectra of GRB 020813 and GRB 021004 using Chandra data. Holland et al. (2002) found no absorption in the vicinity of GRB 021004 (z=2.33) with an upper limit of $N_H = 3.4 \times 10^{21}\mathrm{cm}^{-2}$ using Chandra data.

Mereghetti et al. (2003) found $N_H = 6.8^{+1.8}_{-3.8} \times 10^{22}$ cm^{-2} at $z = 3.9 \pm 0.3$ for GRB 030227 using XMM data. On the other hand, the redshift estimated using the X-ray emission lines is $z = 1.39^{+0.03}_{-0.06}$ (Watson et al. 2003). Considering a possible blueshift from the X-ray emitting plasma, flowing at a velocity of ∼0.1c (Reeves et al. 2002; Butler et al. 2003), the progenitor redshift should be at $z \sim 1.6$. The rest frame column at this redshift would be $N_H = 1.3^{+0.3}_{-0.7} \times 10^{22}$ cm^{-2}.

All these values are in agreement with our rest frame N_H range. We plot the above N_H determinations along with our BeppoSAX measurements in Figure 3.

5.2. Optical-NIR spectral fittings

According to the standard fireball model (see Sari, Piran & Narayan 1998) at >1-2 days from the GRB event, the electron population accelerated by shock mechanisms in a power law energy distribution, is expected to radiate in the so called slow cooling regime. In this regime, if the optical range ν_o is at frequencies higher than the peak of the emission, the spectrum can be well described by a broken power law with indices $\alpha = (p-1)/2$ for $\nu_o < \nu_c$ and $\alpha = p/2$ for $\nu_o > \nu_c$, where ν_c is the cooling frequency and p is the electron energy distribution index. To evaluate the rest frame visual extinction A_{Vr} we fitted the optical to near infrared data with the following model:

$$f(\nu_o) = C\nu_o^{-\alpha} e^{-A(\nu_o(1+z))} \quad (1)$$

where C is the spectral normalization constant, $A(\nu_o(1+z))$ is the rest frame extinction

and z is the GRB redshift.

Since the optical-NIR photometry covers a rather narrow frequency range and the number of independent photometric points for each afterglow is usually small, we could not obtain from the fits strong constraints on *both* the emission spectrum and the rest frame extinction.

We estimated the electronic spectral index p from each X-ray afterglow spectral index $\alpha_X = p/2$ (Tables 5 and 6), assuming that the X-ray frequencies ν_X are above the cooling frequency ν_c (Berger, Kulkarni & Frail 2003). On the basis of the p measures, we then estimated the optical spectral index according to the fireball model (Sari et al. 1998) considering two possible cases, where the optical energy range is below or above the cooling frequency, respectively $\alpha_1 = (p-1)/2$ for $\nu_o < \nu_c$ or $\alpha_2 = p/2$ for $\nu_o > \nu_c$, or b_1, b_2 if the flux is expressed in wavelength (see Tables 7 and 8). We have then estimated the extinction uncertainties taking into account the uncertainties on the estimated optical spectral index b_1 and b_2.

For GRB 000926, that is not included in our X-ray selected sample, we took the electronic spectral index derived from broad band modeling results published in previous works. The interpretation of the broad band spectrum for this burst is not univoque. However, similar values are obtained for the p parameter. Piro et al. (2001) find a best fit model with $\nu_X < \nu_c$, from which the authors derive $p = 2.6 \pm 0.3$. Harrison et al. (2001) adopt a different continuum model with $\nu_c < \nu_o < \nu_X$ and they find a minimum χ^2 for $p = 2.43 \pm 0.06$. Due to the uncertainties on the cooling frequency energy regime, we tested for this afterglow both the possible cases, $\nu_o < \nu_c$ and $\nu_o > \nu_c$, assuming $p = 2.6 \pm 0.3$.

The model in equation (1) has been convolved with the transmission functions of the optical and near infrared filters and then converted into a magnitude using the photometric zero points from Fukugita, Shimasaku & Ichikawa (1995) for the optical range and from Bersanelli, Bouchet & Falomo (1991) for the NIR range. We then compared our results with the observed optical-NIR afterglow SEDs using a χ^2 minimization technique.

Four different extinction curves have been tested and best fit rest frame visual extinction A_{Vr} have been estimated. We used: *i)* the Galactic extinction curve from Cardelli et al. (1989) ("G") assuming $R_V = A_V/E(B-V) = 3.1$; *ii)* the extinction curve of the Small Magellanic Clouds ("SMC") from Pei (1992); *iii)* the extinction curve computed by Calzetti, Kinney & Storchi-Bergmann (1994) and Calzetti (1997) for a sample of local starburst galaxies ("C"); *iv)* the extinction curve computed from simulations by Maiolino, Marconi & Oliva (2001a) based on a dust model skewed toward large grains. The Galactic extinction curve is reasonably well described by a dust model were grain sizes are distributed as a power law,

namely $dn(a) \propto a^q da$, where $n(a)$ is the number density of grains with size $\lesssim a$, $q = -3.5$ and $a_{min} = 0.005\mu\text{m} < a < a_{max} = 0.25\mu\text{m}$ (Mathis, Rumpl & Nordsieck 1977). The Maiolino et al. (2001a) extinction curve Q1 used the same index $q = -3.5$, but a higher maximum grain size $a_{max} = 10\mu\text{m}$.

All these extinction models are plotted in Figure 6.

Note that the Q1 and the C extinction curves are flatter than the rough $\approx \frac{1}{\lambda}$ behavior of the Galactic extinction curve. This gives rise to a more gray extinction. Note also that in the C and in the SMC curves, the 2175 Å hhump is absent, while is quite prominent in the G and Q1 curve.

The origin of this 2175 Å feature is generally interpreted as due to the graphite grains component of the interstellar dust (Mathis 1990). In starburst galaxies the absence of this feature was interpreted to be the effect of a complex geometry for the dust configuration or to a chemical composition different from that of our Galaxy (Calzetti et al. 1994). For the SMC extinction curve, the absence of the 2175 Å hump was explained by a different relative abundances of graphite and silicate grains (Pei 1992).

Strictly speaking, the Calzetti et al. (1994) extinction curve applies to an extended region rather than to a simple line of sight. Nevertheless we think it is instructive to test it because the above mentioned peculiarities of its shape (the absence of the strong 2175 Å hump and the curvature flatter than $\approx \frac{1}{\lambda}$) seems particularly well suited to describe the afterglow optical-NIR SEDs.

The optical extinction is typically quantified by the extinction in the visual band. Tables 7 and 8 give the best fit rest frame visual extinction A_{Vr} and the χ^2 for the two different spectral index values obtained for $\nu_o < \nu_c$ and $\nu_o > \nu_c$ and the four extinction models. In all cases the extinction is assumed at the redshift of the GRB, or at z=1 when the redshift of the GRB is unknown.

In the next Sections individual cases for which interesting results have been obtained from our analysis are discussed.

5.2.1. GRB 010222 and GRB 000926

We found that, for these two afterglows, the C extinction curve provides the best fit model to the optical SED for GRB 000926 and GRB 010222 for $\nu_o < \nu_c$ (Figure 7 and Table 8). The SMC extinction curve provides a fit of quality similar to that obtained with the C model for GRB 010222 while it does not provide a good fit to GRB 000926. Extinction

curves with a strong 2175 Å hump provide an unacceptable fit for these GRB. By comparing the G model with respect to the C model for the case $\nu_o < \nu_c$, we found a probability $P(> \Delta\chi^2)$ of 0.1% for GRB 000926 and $P(> \Delta\chi^2)$ of 0.5% for GRB 010222. We note that these two bursts are those with the widest optical-NIR frequency coverage, which strongly helps in constraining the extinction model.

Lee et al. (2001) find acceptable fits for GRB 010222 assuming the SMC extinction curve with $A_V \sim 0.10$ for $\nu_o > \nu_c$ consistent with our measure (see Table 8). For the same burst, Masetti et al. (2001) obtain acceptable fit over the NIR-optical range using the starburst extinction model, assuming a continuum model different from that one of Lee et al. (2001), for $\nu_o < \nu_c$. Their extinction value is somehow higher but still consistent with the value that we found for the C model with $\nu_o < \nu_c$. Björnsson et al. (2002) derive an optical spectral index of $b = 1.25 \pm 0.03$ for $\nu_o < \nu_c$. We tested the latter spectral index value and we found that it does not affect the result on the C model as the best fitting extinction curve for GRB 010222. Galama et al. (2003) found a rest frame visual extinction value comparable to the Lee et al. (2001) result by using the host galaxy extinction curve model by Reichart (2001).

For GRB 000926 rest frame extinction measured from our analysis are consistent with those of Fynbo et al. (2001), Price et al. (2001) and Harrison et al. (2001) using the Galactic or the SMC extinction curves and their derived spectral index. However, we point out that a better agreement with the data is obtained for this burst with the C extinction curve (see Table 8).

5.2.2. GRB 971214 and GRB 980519

The extinction curve that provides the best fit to the SEDs of these GRB is the SMC model (Figure 8). The statistical improvement with respect to the G model for $\nu_o < \nu_c$, is $\Delta\chi^2 = 13$ for GRB 980519 and $\Delta\chi^2 = 3.6$ for GRB 971214 (with no NIR points), corresponding to a probability $P(> \Delta\chi^2) < 0.1\%$ and $P(> \Delta\chi^2)$ of 7% respectively. We remind that for these two afterglows, the number of photometric points is smaller than for GRB 010222 and GRB 000926 and therefore the constraint on the extinction model is less tight. Moreover, the redshift of GRB 980519 is unknown (we fixed it at z=1). We tested also the redshift as a free parameter. We found that z$\sim$0.7 improves the quality of the fit using the G and Q1 models, because the 2175 Å hump moves out of the observed frequency range. However, the statistical improvement is admittedly low.

For GRB 971214 we tested the hypothesis that the spectral break observed between the optical and NIR bands is due to extinction (Ramaprakash et al. 1998, see §4.3). We found

that the SMC can fit the data (see Figure 8), with A_{Vr} consistent with the extinction value obtained for the same model fitting only the V, R and I points. By comparing the G model with respect to the SMC model for $\nu_o < \nu_c$, we found a probability $P(> \Delta\chi^2)$ of 3%.

5.2.3. GRB 970508

GRB 970508 is the only case for which the extinction curves including a strong 2175 Å hump (G and the Q1) provide a good fit to the data (see Table 7). However, the C and SMC models provide only slightly higher χ^2.

5.2.4. GRB 980329

The redshift of GRB 980329 is unknown, puzzling the interpretation of the sharp break between the R and I points observed in its SED (e.g. Palazzi et al. 1998, Reichart et al. 1999b). This spectral jump has been explained in terms of Lyα absorption from neutral hydrogen along the line of sight to a high redshift source ($z > 5$ Fruchter et al. 1999b). However, Yost et al. (2002) suggested that such a high redshift is not compatible with the GRB host galaxy colors. The sharp break between the R and the I band may be due to the presence of a strong 2175 Å hump opportunely redshifted. Indeed, although the χ^2 are still not acceptable, we found a minimum χ^2 at $z = 1.8 \pm 0.1$ by using the Galactic extinction curve (Figure 9). A similar analysis has been performed by Lamb, Castander & Reichart (1999) on the broad band, from radio to X-ray SED and they obtained a qualitatively similar result. These values are consistent with the redshift range found by Jaunsen et al. (2003) that excluded at 95% confidence level $z > 4.2$ and $z < 1.2$. The latter authors found an host galaxy photometric redshift of z$\sim$ 3.6.

5.2.5. GRB 970228, GRB 980519, GRB 990123 and GRB 990510

We found that, for these afterglows, best fit spectral models are consistent with null extinction for both the two tested spectral indexes.

The lack of extinction for these afterglows will put severe constraints on the estimation of the dust to gas ratio in GRB environment (see next Section), especially the case of GRB 990510, for which a significant N_H column density has been detected.

A dedicated spectral analysis of the bright GRB 990123 has been previously performed

by Galama et al. (1999), Andersen et al. (1999) and Holland et al. (2000). They found spectral index values of $b = 1.33 \pm 0.02$ (from optical to X-ray spectrum), $b = 1.250 \pm 0.068$ (from a weighted mean over temporal scansion of the optical spectrum) and $b = 1.31 \pm 0.10$ respectively, and an extinction consistent with zero. We tested their spectral indexes in our analysis and we obtain similar results.

5.3. N_H versus A_{Vr}

Figures 10, 11 and 12 compare the best fit additional column densities at the redshift of the GRB (see previous Section) with best fit A_{Vr} obtained with the spectral index b_1, corresponding to the case $\nu_o < \nu_c$ (see Tables 7 and 8) and assuming three different extinction curves.

In the case of Galactic extinction curve (Figure 10), several GRB lie well above the N_H versus A_{Vr} relationship expected if a Galactic dust to gas mass ratio is assumed. The same analysis was performed with spectral index b_2, corresponding to the case $\nu_o > \nu_c$ and the obtained best fit extinction values are in this case even lower than in the previous case (Tables 7 and 8). The solid curve in Figure 10 is the relationship estimated by Predehl & Schmitt (1995) between N_H and A_{Vr}: $N_H = A_{Vr} \times 1.8 \times 10^{21}$ cm^{-2}. We performed a χ^2 test to compare the rest frame N_H values (for those afterglows at known redshift) to those predicted by the observed extinction A_{Vr} based on this relationship, and we obtained $\chi^2 = 12.1$ for 5 d.o.f. (probability P($> \chi^2$) of 3.5%).

This behavior has been seen in other cosmic sources like AGN as can be seen from the open squares in Figure 10 (from a compilation of Maiolino et al. 2001b and Elvis et al. 1998). It appears that GRB are similar to AGN in their N_H/A_{Vr} ratio, although AGN show somewhat higher N_H and A_{Vr}.

A good agreement between measured N_H and A_{Vr} is obtained using the SMC model, since for the SMC, the N_H/A_{Vr} ratio is roughly one order of magnitude higher than the Galactic case and is $N_H/A_{Vr} = 1.6 \times 10^{22}$ cm^{-2} (Weingartner & Draine 2001). We performed a χ^2 test to compare the rest frame N_H values (for those afterglows at known redshift) to those predicted by the observed extinction A_{Vr} and we obtained $\chi^2 = 7.0$ for 5 d.o.f. (probability P($> \chi^2$) of 25%, Figure 11). We note, however, that in estimating the column densities from the X-ray absorption, a metallicity lower than the Galactic one should have been considered if we hypothize a SMC-like environment (Pei 1992). To reproduce the energy cut-off in the X-ray afterglow spectra with a metallicity $\sim 1/8$ of the solar one, an hydrogen column density increased by a factor of ~ 7 is required. We measured the rest frame column densities with a

chemical abundance $\sim 1/8$ of the solar one and we compared them to those predicted by the observed extinction A_{Vr}. We found that the χ^2 increases by 24.1, with $P(> \Delta\chi^2) < 0.001$.

A better result is obtained using the Q1 extinction curve. For this latter model the N_H/A_{Vr} ratio is 7.1×10^{21} cm^{-2} (Maiolino et al. 2001a) for a solar metallicity, thus providing a self consistent solution. The χ^2 obtained by comparing the measured N_H to those predicted by the observed A_{Vr} is $\chi^2 = 5.4$ for 5 d.o.f. (probability P($> \chi^2$) of 35%, Figure 12). We note that the Q1 model does not usually provide good fits to the observed optical-NIR SEDs, because of the presence of a strong 2175 Å hump (see Figure 6). However, it seems that this is the model that can better explain the measured N_H/A_{Vr} values. This is due to the flat shape of this extinction curve that gives a more gray extinction than the Galactic or SMC cases and to the high N_H/A_{Vr} ratio.

The C extinction curve has a similar shape to Q1 (see Figure 6) and no strong 2175 Å hump. Unfortunately, the N_H/A_{Vr} ratio has not been estimated for the starburst galaxies, because of the complexity of the geometry of the dust and stars distribution inside these galaxies (Calzetti 2001). Therefore, we cannot test the data against the prediction of this model.

5.3.1. Test of the fireball model

As discussed in section 5.2 the continuum spectral index adopted in the optical-NIR photometry fits was derived from the best fit X-ray spectral index, assuming the fireball model, and assuming that the X-ray frequencies are above the cooling frequency. We have performed a selfconsistency check of these assumptions by plotting the afterglow NIR to X-ray SED, after correction for dust extinction and gas absorption, along with the best fit X-ray power law model and the assumed optical power law model. The normalization of the X-ray spectra has been scaled to the same time of the optical-NIR observations, using the published decay indices. We note that in most cases (but GRB 970228 and GRB 970508) the X-ray observations encompass the times at which the optical-NIR observations were performed, see Table 3 and 4, thus minimizing any systematic uncertainty in the scaling of the X-ray spectra. Figure 13 shows three examples: GRB 990123, GRB 990510 and GRB 010222, which are among the brightest of our sample. In these three cases the optical-NIR photometry has been corrected for rest frame extinction using the best fit value relative to the Q1 model, or its upper limit when it is consistent with zero. Similar results are obtained using the C model. Note as using these extinction laws the optical and X-ray spectra of GRB 010222 are consistent with the fireball model. Adopting the G and the SMC extinction laws, or no extinction, we find again the result already reported by in't Zand et al. (2001).

Figure 13 show that the NIR to X-ray SEDs are well consistent with the fireball model, and that the cooling frequency is constrained within the UV and the X-ray band. Qualitatively similar results are found also for the other afterglows. We remark, however, that in latter cases this is not a truly stringent test, given the lower statistics in the X-ray spectra and the consequent larger uncertainties on the X-ray spectral index, (and therefore also in the allowed range of values for the optical index).

6. Discussion

6.1. X-ray analysis

We analyzed the X-ray absorption properties of a sample of 13 bright GRB afterglows observed by BeppoSAX in the energy range $0.1(0.4) - 10.0$ keV. We found that absorption in addition to the Galactic one along the line of sight is highly statistically significant in two cases: GRB 990123 and GRB 010222 (probability $> 99.9\%$). These are also the two GRB with the best statistics. However, fitting the spectra of two other GRB afterglows with lower but still reasonably good statistics (GRB 971214 and GRB 970228), including an additional absorber does not produce a significant improvement in χ^2 (probability of 93.3% and 90.8% respectively). In three other cases (GRB 980703, GRB 990510 and GRB 001109) the presence of an additional absorber is marginally significant (probability $\sim 97\%$). X-ray absorption may be common, although the quality of present data does not allow us to reach a firm conclusion. In all cases, the absorbing columns at the GRB redshift are in the range $N_H = 10^{21}$ - a few $\times 10^{22}$ cm^{-2}, values similar to the column usually observed toward the disk and the bulge of the Galaxy, suggesting that GRB afterglows are probing similar environments in the GRB host galaxies. This range is also in agreement with the estimation of the N_H expected if GRB were embedded in giant molecular clouds similar to those observed in our galaxy (Reichart & Price 2002).

De Pasquale et al. (2003) performed an analysis on the BeppoSAX X-ray afterglows, aimed at studying the nature of Dark GRB (for which no or very faint optical counterpart has been discovered). Their conclusions from column density measures are generally consistent with those given in this paper.

The rest frame column density estimated for 9 X-ray afterglows observed by XMM (GRB 011211, GRB 020322 and GRB 030227) and Chandra (GRB 991216, GRB 000210, GRB 000926, GRB 020405, GRB 020813 and GRB 021004) are consistent within the range found for the 13 BeppoSAX GRB (see Figure 3).

The spectrum of GRB 010222 suggests the presence of complex absorber or an addi-

tive emission component (Figure 5). Two possible explanations invoke the recovery of the spectrum below the energies of strong ionized absorption edge lines as OVII, OVIII or the spilling of the emission spectrum through a leaky absorber. We tested both models obtaining a significant improvement of the χ^2 in both cases (Figure 5). We found an upper limit to the equivalent width of a line at 6.4/(1+z) keV of 150(1+z) eV (90% confidence level), that is, one order of magnitude smaller than the line equivalent width measured for GRB 000214 (Antonelli et al. 2000).

6.2. Optical-NIR SEDs fitting

We evaluated the rest frame visual extinction of the nine optical afterglows in our sample. In addition we analyzed also the optical afterglow of GRB 000926 (see §5.2.1).

We fitted the optical-NIR afterglows photometry with a power law model modified at short wavelengths by rest frame extinction (see equation (1) in §5.2). We tested four different extinction curves: *i)* Galactic ("G"); *ii)* Small Magellanic Clouds ("SMC"); *iii)* the extinction curve computed for a sample of local starburst galaxies ("C"); *iv)* an extinction curve computed from simulations by Maiolino et al. (2001a) based on a dust distributions skewed toward large grains ("Q1").

In two cases, GRB 010222 and GRB 000926, we found that the extinction curve that better fit the data is the C model. These afterglows have the widest optical-NIR frequency coverage in our sample. This strongly help in constraining the extinction model. In particular, those extinction curves with a strong 2175 Å hump (G and Q1) are not suitable to model these two afterglows. In fact, despite Q1 has a slope very similar to that of the C model (see Figure 6), it fails to fit their optical SEDs due to the presence of a strong 2175 Å hump that, on the other hand is completely absent in the C curve.

We note that assuming the C or the Q1 model, the NIR to X-ray SED of GRB 010222 is fully consistent with the fireball model, without the need of a strong contribution from inverse Compton scattering in the X-ray band (see eg. in't Zand et al. 2001).

The SMC model provides good fit to the GRB 980519 and GRB 971214 data (by using for the latter both optical and NIR data, see §5.2.2). However, the number of photometric points is smaller than for GRB 010222 and GRB 000926 and therefore the constraint on the extinction model is less tight. Moreover, the redshift of GRB 980519 is unknown and for GRB 971214 the interpretation of the spectral break observed between the optical and NIR bands is not univoque (see §4.3). Excluding the NIR points, both the SMC and the C extinction curves provide comparable good fit to GRB 971214.

The small curvatures of the GRB 990510 and GRB 990123 SEDs require very low extinction. No strong constraints on the extinction model can be obtained also in the cases of GRB 970228 and GRB 980329 because of the few photometric points.

6.2.1. The 2175 Å hump

The extinction models tested in our analysis that have a strong 2175 Å hump are indicated as G and Q1 (see §5.2 and Figure 6).

We found that in all the analyzed optical-NIR SEDs, except GRB 970508, the G and Q1 model give bad χ^2 (see Table 8).

This 2175 Å hump does not appear to be a common feature in extra galactic sources (Calzetti et al. 1994) and there is not yet a clear and univoque interpretation of its absence. In the case of GRBs, the absence of the 2175 Å can be explained by the results obtained by Perna et al. (2002b). They find that dust destruction of the small graphite grains due to an intense X-ray/UV source, as could be for GRB, would produce a significantly suppression of the 2175 Å hump.

Two bursts in our sample are at unknown redshift: GRB 980519 and GRB 980329. We found that for GRB 980519, a lower redshift (z$\sim$0.7) improves, although not very significantly, the quality of the fit using the G and Q1 models, because the 2175 Å hump moves out of the observed frequency range. For GRB 980329, the jump between the R and I photometric points is marginally explained by the 2175 Å hump redshifted to the optical range (z$\sim$1.8, see Figure 9).

6.3. N_H versus A_{Vr} relationship

As discussed in the previous sections, we have evaluated rest frame optical extinction A_{Vr} from the optical to near infrared photometry and rest frame equivalent hydrogen column densities N_H from the X-ray data.

We found that several GRB lie well above the N_H versus A_{Vr} relationship expected for the Galactic extinction curve (Figure 10). In this regard our results are qualitatively similar to those of Galama & Wijers (2001), although the best fit N_H values are somewhat smaller than those reported by the latter authors, and visual extinction are evaluated here using detailed extinction curves (while Galama & Wijers (2001) assume a linear extinction curve $A(\lambda) \propto \frac{1}{\lambda}$ and computed rest frame N_H by using a simple power law scaling of the N_H

measured in the observer frame).

Scenarios that can reconcile the observed X-ray absorption with the lack of strong optical extinction, involve the presence of a dust to gas ratio much lower than the Galactic one (see Figure 6), and/or of a dust grain size distribution skewed toward large grains. We discuss these two possibilities in turn.

A dust to gas ratio much lower than the Galactic one has been tested assuming the SMC extinction curve. In fact, for the SMC ISM it has been inferred a dust content $\sim 1/10$ of the Galactic one (Pei 1992). A good agreement between the best fit N_H and A_{Vr} is obtained using this extinction curve (Figure 11). We note, however, that the best fit N_H values have been obtained by assuming Galactic metal abundances, while the metallicity of the SMC ISM is $\sim 1/8$ the Galactic one (Pei 1992). If such low metallicity were assumed, best fit N_H values became ≈ 7 times higher than those quoted in Tables 5 and 6 as plotted in Figure 11 (dashed line), worsening the agreement with the best fit optical extinction. We can therefore conclude that also for an SMC-like ISM the observed extinction is significantly lower than predicted from the X-ray column density.

Large grains give gray opacity from optical to the infrared (e.g. Kim, Martin & Hendry 1994, Weingartner & Draine 2000, Maiolino et al. 2001a), that could explain the small curvature observed in the optical afterglow SEDs. A low A_V/N_H supports the scenario were large grains are formed by coagulation mechanisms (e.g. Kim & Martin 1996, Maiolino et al. 2001a). Since the grain coagulation rate increases with density as $n^{1/2}$ (Draine 1985), the depletion of small grains by coagulation mechanisms is expected to be particularly efficient in high density environments, as the giant molecular clouds which could harbor GRB events.

High density gas and dust coagulation is not the only viable mechanism to produce a dust grain size distribution skewed toward large grains. If the dust to metal ratio is constant, as in the Galaxy and the two Magellanic Clouds ISM (Pei 1992), the lack of strong extinction (dust), along with a consistent amount of X-ray absorption (metal), suggest a scenario were dust is destroyed by the intense GRB X-ray/UV flux. Dust grains may be heated and evaporated by the intense X-ray and UV radiation field up to $\sim 20pc$ (Waxmann & Draine 2000, Draine & Hao 2002, Fruchter, Krolik & Rhoads 2001). Perna et al. (2002b) and Perna & Lazzati (2002c) show that the result of the exposure of dust to the intense GRB radiation field can be a grain size distribution flatter that the original one. The main reason is that dust destruction is more efficient on small grains. Perna et al. (2002b) computed the extinction curve which is obtained if standard Galactic dust is exposed to a GRB, and found that the dust extinction curve can be very flat, at least for burst lasting more than a few tens of seconds.

We tested a dust model skewed toward large grains using the model Q1 adapted from Maiolino et al. (2001a). The X-ray N_H agree very well with the hydrogen column density expected from the best fit A_{Vr} and the visual extinction-reddening ratio appropriate for this model (see Figure 12). We note that this model does not imply a metallicity lower than solar, thus providing a self consistent solution, unless the SMC-like ISM.

However, the Q1 curve gives generally worse χ^2 (see Table 7 and 8) than the SMC and C models. This is mainly due to the presence of a strong 2175 Å hump in the Q1 model. The C extinction curve has a slope similar to that of the Q1 model (Figure 6), but no 2175 Å hump, thus providing better fits. This difference does not affect the rest frame extinction estimates, whose values from both models are indeed comparable (see Table 7 and 8) and suggests that an extinction model with a "flat" slope and no 2175 Å hump would produce both good fits to most observed SEDs and a nice agreement between N_H and A_{Vr}.

In the near future we will have the chance to confirm this intriguing scenario. *Swift* will enable us to obtain high quality X-ray spectra of the afterglow as a function of the time. The *Swift* optical monitor will allow us to obtain precise and reliable optical-UV photometry. Robotic telescopes like REM, triggered by *Swift*, will be able to obtain simultaneous near infrared photometry. Therefore it will be possible to obtain precise reddening measures, constraining the correct extinction law, and to follow the evolution of the reddening as a function of the time, that is the smoking gun of a possible GRB UV/X-ray flux influence on their environment.

This research has been partially supported by COFIN 2001 grants, by CNAA 1999 and 2000 grants and by University of Rome "La Sapienza" support.

We would like to thank Roberto Maiolino for his precious support to this work, Rosalba Perna, Sandra Savaglio, Daniela Calzetti, Nicola Masetti for useful discussions and an anonymous referee for corrections that improved the presentation. BeppoSAX was a program of the Italian Space Agency (ASI) with participation of the Dutch space agency (NIVR). We would like to thank all the members of the BeppoSAX team for the support in performing observations with the satellite. We also thank an anonymous referee for comments that helped in improving this presentation.

REFERENCES

Ahn, S. 2000, ApJ, 530, 9

Amati, L., et al. 2000, Science, 290, 953

Andersen, M.I. et al. 1999, Science, 283, 2075

Andersen, M.I. et al. 2000, A&A, 364, L54

Antonelli, L.A. et al. 2000, ApJ, 545, 39

Ballantyne, D.R., Ramirez-Ruiz, E., Lazzati, D. & Piro, L. 2002, A&A, 389, L74

Berger, E., Kulkarni, S.R. and Frail, D.A., 2001, ApJ, 560, 652

Berger, E., Kulkarni, S.R. and Frail, D.A., 2003, ApJ, 590, 379

Bersanelli, M., Bouchet, P. & Falomo, R. 1999, A&A, 252, 854

Beuerman, K. et al. 1999, A&A, 352, L26

Bevington, F.R. & Robinson, D.K. 1992, Data reduction and error analysis for the physical sciences, Second Edition (WCB; Mc-Grow Hill)

Björnsson G. et al. 2002, ApJ, 579, L59

Bloom, J.S., et al. 1998a, ApJ, 508, L21

Bloom, J.S., Djorgovski, S.G. & Kulkarni, S.R. 1998b, ApJ, 507, 25

Bloom, J.S., et al. 1999, ApJ, 518, L1

Bloom, J.S., Djorgovski, S.G. & Kulkarni, S.R. 2001, ApJ, 554, 678

Bloom, J.S., Kulkarni, S.R. & Djorgovski, S.G. 2002a, AJ, 123, 1111

Bloom, J.S., et al. 2002b, ApJ, 572, L45

Boella, G. et al. 1997b, A&AS, 122, 327

Böttcher, M., Dermer, C.D., Crider, A W. & Liang, E.P. 1999, A&A, 343, 111

Borozdin, K.N. & Trudolyubov, S. P. 2003, ApJ, 583, L57

Butler, N.R. et al. 2003, ApJ, 597, 1010

Calzetti, D., Kinney, A.L. & Storchi-Bergmann, T. 1994, ApJ, 429, 582

Calzetti, D. 1997, AJ, 113, 1

Calzetti, D. 2001, PASP, 113, 1449

Cardelli,J.A., Clayton,G.C. & Mathis,J.S. 1989, ApJ, 345, 245

Castander, F.J. & Lamb, D. 1999, ApJ, 523,602

Castro, S. et al. 2003, ApJ, 586, 128

Castro-Tirado, A.J., et al. 1999, ApJ, 511, L85

Chiappetti L. et al. 1998, Nucl. Phys. B (Proc. Supp.), 69/103, 610

Ciardi, B. & Loeb 2000, ApJ, 540, 687

Costa, E., et al. 1999, A&AS, 138, 425

Cowsik,R. et al. 2001, Bull. Astr. Soc. India, 29, 157

de Vries, H.W., Heithausen, A. & Thaddeus, P. 1987, ApJ, 319, 723

De Pasquale, M., et al. 2003, ApJ, 592, 1018

Della Valle, M. et al. 2003, A&A, 406, 33

Djorgovski, S.G. et al. 1997, Nature, 387, 876

Djorgovski, S.G. et al. 1998a, ApJ, 508, L17

Djorgovski, S.G., Kulkarni, S.R., Bloom, J.S., Goodrich, R., Frail, D.A. 1998b, ApJ, 508, L17

Djorgovski, S.G., Kulkarni, S.R., Bloom J.S. & Frail, D.A. 1999, GCN Circ. 289

Djorgovski, S.G. et al. 2001, proc. "Gamma-Ray Bursts in the Afterglow Era: 2nd Workshop", Edited by Enrico Costa, Filippo Frontera, and Jens Hjorth. Berlin Heidelberg: Springer, 2001, 218

Draine, B.T. 1985, Protostars and Planets II, ed. D.C.Black & M.S.Matthews, Sp. Sc. Ser. (The Univ. of Arizona Pr.)

Draine, B.T., & Hao, L. 2002, ApJ, 569, 780

Dickey, J.M. & Lockman, F.J. 1990, ARA&A, 28, 215

Eichler, D., Livio., M., Piran, T. & Shramm, D.N. 1989, Nature, 340, 126

Elvis, M., Lockman, F.J. & Wilkes, B.J. 1989, AJ, 97, 777

Elvis, M., Fiore, F., Giommi, P. & Padovani, P. 1998, ApJ, 492, 91

Fiore, F., Guainazzi, M. & Grandi, P. 1999, *Handbook for BeppoSAX NFI spectral analysis*, ftp://www.sdc.asi.it/pub/sax/doc/software_docs/saxabc_v1.2.ps.gz

Fiore, F., Nicastro, F., Savaglio, S., Stella, L. & Vietri, M. 2000 ApJL, 544, L7

Fiore, F. 2001, Proceeding of 'New Century of X-ray Astronomy', Yokohama, Japan, astro-ph/[0107276]

Fox, D.W., et al. 2003, Nature, 422, 284

Frail, D.A. et al. 2002, ApJ, 565, 829

Frail, D.A. et al. 2003, ApJ, 590, 992

Frontera, F., Costa, E., dal Fiume, D., Feroci, M., Nicastro, L., Orlandini, M., Palazzi, E. & Zavattini, G. 1997, A&AS, 122, 357

Frontera, F., et al. 2000, ApJS, 127, 59

Fruchter, A.S. et al. 1999a, ApJ, 516, 683

Fruchter, A.S. 1999b, ApJ, 562, 683

Fruchter, A.S., Krolik, J.H., & Rhoads, J.S. 2001, ApJ, 563, 597

Fryer, C.L., Woosley, S.E. & Hartman, D.H. 1999, AJ, 526, 152

Fukugita, M., Shimasaku, K. & Ichikawa, T. 1995, PASP, 107, 945

Fynbo J.P.U. et al. 2001, A&A, 373, 796

Galama, T.J. et al. 1997, Nature, 387, 479

Galama, T.J. et al. 1998a, ApJ, 497, 13

Galama, T.J., Wijers, R.A.M.J., Bremer, M., Groot,P.J., Strom, R.G., Kouveliotou, C. & Van Paradijs, J. 1998b, ApJ, 500, 97

Galama, T.J., et al. 1999, Nature, 398, 394

Galama, T.J. et al. 2000, ApJ, 536, 185

Galama, T.J., & Wijers, A.M.J. 2001, ApJL, 549, L209

Galama, T.J. et al. 2003, ApJ, 587, 135

Garcia, M.R. et al. 1998 ApJ, 500, L105

Ghisellini, G., Lazzati, D., Rossi, E. & Rees, M.J. 2002, A&A, 389, L33

Gonzalez, R.A., Fruchter, A.S. & Dirsch, B. 1999, ApJ, 515, 69

Gorosabel, J. et al. 1998, A&A, 335, L5

Greiner, J. et al., CGN Circ. 2020

Guarnieri, A. et al. 1997, A&A, 328,L13

Halpern, J.P., Thorstensen, J.R., Helfan, D.J. & Costa, E. 1998, Nature, 393, 41

Halpern, J.P., Kemp, J. & Piran. T. 1999, ApJ, 517, L105

Harrison, F.A., et al. 1999, ApJ, 523, L121

Harrison, F.A., et al. 2001, ApJ, 559, 123

Heiles, C., Reach, W.T. & Koo, B.-C. 1988, ApJ, 332, 313

Henden, A.A. et al. 1998, GCN Circ. 131

Hjorth, J. et al. 2003, Nature, 423, 847

Holland,S., Björnsson,J., Hjorth,J. Thomsen,B. 2000 A&A, 364, 467

Holland, S. et al. 2001, A&A, 371, 52

Holland, S. et al. 2002, AJ, 124, 639

Jha, S. et al. 2001, ApJ, 554, L155

Jaunsen, A.O. et al. 2001, ApJ, 546, 127

Jaunsen, A.O. et al. 2003, A&A, 402, 125

in't Zand, J.J.M. et al. 2001, ApJ, 559, 710

Kawabata, K.S., et al. 2003, ApJ, 593, 19

Kim, S.-H., Martin, P.G. & Hendry, P.D. 1994, ApJ, 422, 164

Kim, S.-H. & Martin, P.G. 1996, ApJ, 462, 296

Kulkarni, S.R., et al. 1998, Nature, 393, 35

Kulkarni, S.R., et al. 1999, Nature, 398, 389

Kumar, P. & Narayan, R. 2003, ApJ, 584, 895

Lamb, D.Q., Castander, F.J. & Reichart, D.E. 1999, A&ASS, 138, 479

Laureijs, R.J. 1989, Ph.D.thesis, Groningen University

Laureijs, R.J., Helou, G. & Clark, F.O. *The First Symposioum on the Infrared Cirrus and Diffuse Interstellar Clouds* (edsCutri,R. & Latter,W.) 133-136 (Conf. Ser. 58, Astron. Soc. Pacific., Provo, UT, 1994)

Lazzati, D., Covino, S. & Ghisellini, G. 2002a, MNRAS, 330, 583

Lee B.C. et al. 2001, ApJ, 561, 183

MacFayden, A. & Woosley, S.E. 1999, ApJ 524,262

Maiolino, R., Marconi, A., & Oliva, E. 2001a, A&A, 365, 37

Maiolino, R., Marconi, A., Salvati, M., Risaliti, G., Severgnini, P., Oliva, E., La Franca, F. & Vanzi, L. 2001b, A&A, 365, 28

Manzo, G., Giarrusso, S., Santangelo, A., Ciralli, F., Fazio, G., Piraino, S. & Segreto, A. 1997, A&AS, 122, 341

Masetti, N.,et al. 2001, A&A, 374, 382

Mathis, J. S., Rumpl, W. & Nordsieck, K. H. 1977, ApJ, 217, 425

Mathis, J.S. 1990, ARA&A, 28, 37

Mereghetti, S. et al. 2003, ApJ, 590, 73

Meszaros, P. & Rees, M.J. 1992, ApJ, 397, 570

Mirabal, N. et al. 2002a, ApJ, 578, 818

Mirabal, N., Paerels, F. & Halpern, J.P. 2002b, ApJ, 587, 128

Mirabal, N. et al. 2002c, ApJ, 578, 818

Narayan, R., Paczynski, B. & Piran, T. 1992, ApJ, 395, L83

Norris,J., Scargle,J. & Bonnell, J. 2000, BAAS, 32, 1244

Odewahn, S.C., et al. 1998, ApJ, 509, 5

Paczynski, B. 1998, ApJL, 494, L45

Paczynski, B. 1990, ApJ, 348, 485

Palazzi, E. et al. 1998, A&A, 336, L95

Parmar A., et al. 1997, A&AS, 122, 309

Pedersen, H. et al. 1998, GCN Circ. 142

Pedichini, F. et al. 1997, A&A, 327, L36

Pei, Y.C. 1992, ApJ, 395, 130

Perna, R. & Loeb, A. 1998, ApJ, 501, 467

Perna, R. & Belczynski, K. 2002a, ApJ, 570, 252

Perna, R., Lazzati, D. & Fiore, F. 2002b, ApJ, 585, 775

Perna, R. & Lazzati, D. 2002c, ApJ, 580, 261

Pettini, M., Smith, L.J., King, D.L. & Hunstead, W. 1997, ApJ, 486, 665

Pettini, M., Ellison, S.L., Steidel, C.C. & Bowen, D.V. 1999, ApJ, 510, 576

Piro, L. et al. 1999, ApJL, 514, L73

Piro, L., et al. 2000, Science, 290, 955

Piro, L., et al. 2001, ApJ, 558, 442

Piro, L. 2002a, proc. "Gamma-Ray Bursts in the Afterglow Era: 3nd Workshop", in press

Piro, L., et al. 2002b, ApJ, 577, 680

Price, P.A. et al. 2001, ApJ, 549, L7

Price, P.A. et al. 2003, Nature, 423, 844

Predehl, P. & Schmitt, J.H.M.M. 1995, A&A, 293, 889

Ramaprakash, A.N., et al., 1998, Nature, 393, 43

Reach, W.T., Heiles, C. & Koo, B.-C. 1993, ApJ, 412, 127

Reeves, J.N. et al. 2002, Nature, 416, 512

Reichart, D. E. 1997, ApJ, 485, L57

Reichart, D. E. 1998, ApJ, 495, 99

Reichart, D. E. 1999a, ApJ, 521, 111

Reichart, D. E., et al. 1999b, ApJ, 517, 692

Reichart, D. E. 2001, ApJ, 553, 235

Reichart, D. E. & Price, P.A. 2002, ApJ, 565, 174

Rhoads, J. et al. 1998, GCN Circ. 144

Rowan-Robinson, M. et al. 1991, MNRAS, 249, 729

Sahu, K. et al. 1997, Nature, 387,476

Sari, R., Piran, T. & Narayan, R. 1998, ApJL, 197, L17

Savage, B.D. & Mathis, J.S. 1979, ARA&A, 17, 73

Savaglio, S., Fall, M., & Fiore, F. 2003, ApJ, 585, 638

Schlegel, D.J., Finkbeiner, D.P. & Davis, M. 1998, ApJ, 500, 525

Simon, V., Hudec, R., Pizzichini, G. & Masetti, N. 2001, A&A, 377, 450

Stark, A.A. et al. 1992, ApJS, 79, 77

Sokolov, V.V., Kopylov, A.I., Zharikov, S.V., Feroci, M., Nicastro, L. & Palazzi, E. 1998a, A&A, 334, 117

Sokolov, V.V. et al. 1998b, GCN Circ. 147

Stanek, K.Z., Garnavich,P.M., Kaluzny,J., Pych,W., Thomson,I. 1999, ApJ, 522, 39

Stanek, K.Z. et al. 2003, ApJ, 591L, 17

Steidel, C. et al. 1999, ApJ, 519, 1

Vietri, M. & Stella, L. 1998, ApJ, 507, L45

Vreeswijk, P.M., et al. 1999, ApJ, 523, 171

Vreeswijk, P.M., et al. 2000, ApJ, 546, 672

Watson, D., Reeves, J.N., Osborne, J.P., Tedds, J.A., O'Brien, P.T., Tomas, L. & Ehle, M. 2002, A&A, 395, L41

Watson, D., Reeves, J.N., Hjorth, J., Jakobsson, P. & Pedersen, K. 2003, ApJ, 595, 29

Waxman, E., & Draine, B. T. 2000, ApJ, 537, 796

Weingartner. J.C. & Draine, B.T. 2000, AAS, 197, 4207

Weingartner. J.C. & Draine, B.T. 2001, ApJ, 548, 296

Wijers, R.A.M.J. & Galama, T.J. 1999, ApJ, 523, 177

Woosley, S. E. 1993, ApJ, 405, 273

Yoshida, A. et al., 1999, A&AS, 138, 433

Yost, S.A. et al. 2002, ApJ, 577, 155

Zapatero Osorio, M.R. et al. 1998, IAU Circ. 6967

A. Appendix

GRB 970228: A large number of papers report photometric observations of the optical afterglow of GRB 970228 (e.g. Guarnieri et al. 1997, Sahu et al. 1997, Galama et al. 1997, Reichart 1997, Pedichini et al. 1997, Garcia et al. 1998, Castander & Lamb 1999, Fruchter et al. 1999a, Reichart 1999a, Galama et al. 2000). The latter paper presents a complete and exhaustive summary of the available optical observations, and therefore we refer to this paper for this afterglow. The Galactic extinction in the direction of GRB 970228 is $A_V = 0.78 \pm 0.12$, from the SFD maps. Castander & Lamb (1999) estimate a Galactic extinction of $A_V = 1.09^{+0.10}_{-0.20}$ combining the results of four different methods for measuring the extinction (also see Fruchter et al. 1999a, and Gonzalez, Fruchter & Dirsch 1999). We used both these values and we verified that their difference does not affect significantly the estimation of the rest frame extinction.

GRB 970508: Galama et al. (1998a) collect observations over the entire optical band, from U to I, for this afterglow, and therefore we referred to this paper in this case. Different authors have reported different estimates of the Galactic extinction in the direction of GRB 970508. Galama et al. (1998a) report $A_V < 0.01$ (Laureijs 1989), while Djorgovski et al. (1997) report $A_V = 0.08$ (Laureijs, Helou & Clark 1994), both using the 100μm cirrus flux maps. Reichart (1998) reports $A_V = 0.09$, using the Rowan-Robinson et al. (1991) maps (also see Sokolov et al. 1998a, Galama et al. 1998b, Bloom, Djorgovski & Kulkarni, 1998a, Castro-Tirado & Gorosabel 1999). We adopt here the value found by the two latter authors.

GRB 971214: We refer to the Ramprakash et al. (1998) work that report K-band magnitudes and collect previous V, R, I, J observations (Gorosabel et al. 1998, Odewahn et al. 1998, Wijers & Galama 1999, Ahn 2000) for this burst. The Galactic extinction in the direction of this burst is negligible (Halpern et al. 1998). A strong spectral curvature is evident in Figure 1 for this afterglow. Wijers & Galama (1999) interprets this feature as due to a genuine break in the emission spectrum, expected in the blast wave model when the cooling frequency is in the optical range (Galama & Wijers 2001 exclude for this reason the NIR data from their analysis, when trying to determine the rest frame extinction fitting the SED with a simple power law). On the other hand, Halpern et al. (1998) and Ramaprakash et al. (1998) interpret the spectral curvature in terms of extinction by intervening dust. They point out that a simple $A_\lambda \propto 1/\lambda$ dust extinction law does not fit properly the data and that a more complex extinction law should be considered. In the following we consider both possibilities.

GRB 980329: We take the photometric data from the work of Reichart et al. (1999b) which present an extended and complete summary of all the observations of this burst (but see also Palazzi et al. 1998). The Galactic reddening in the direction of GRB 980329 is estimated as E(B-V)=0.073 mag using the SFD maps.

GRB 980519: We take the photometric data from the work of Jaunsen et al. (2001). Halpern et al. (1999) report two different values for the Galactic reddening: E(B-V)=0.267 using the SFD maps and E(B-V)=0.348 using the 21 cm Stark et al. (1992) maps and assuming a standard N_H to $E(B-V)$ conversion (Savage & Mathis 1979). Jaunsen et al. (2001) find E(B-V)=0.24 using an alternative method, similar to the SFD determination. We adopt here the latter value.

GRB 980703: The first observations of this afterglow were performed in the NIR band some ∼30 hours after the GRB event. Later optical observations are strongly affected by the host galaxy emission. We considered here only the NIR points from the work of Vreeswijk et al. (1999) which summarize most previous observations (Zapatero Osorio et al. 1998, Rhoads et al. 1998, Henden et al. 1998, Bloom et al. 1998a, Pedersen et al. 1998, Djorgovski et al.

1998a, Sokolov et al. 1998b, Castro-Tirado et al. 1999, but also see Berger, Kuulkarni & Frail 2001, Holland et al. 2001, Frail et al. 2003). The Galactic extinction in the direction of GRB 980703 is $A_V = 0.19$, using the SFD maps.

GRB 990123:

The optical and infrared observations of this afterglow, (Bloom et al. 1999, Holland et al. 2000), are well summarized by Galama et al. (1999) and by Kulkarni et al. (1999) and therefore we took the photometric data from these two works. The Galactic extinction in the direction of GRB 990123 is $A_V = 0.053$, using SFD maps.

GRB 990510: We took the B, V, R, I photometry from the work of Stanek et al. (1999) (but also see Harrison et al. 1999, Beuerman et al. 1999 and Holland et al. 2000), which gives a complete summary of the optical observation on this burst. These authors report magnitudes already corrected for the Galactic reddening E(B-V)=0.203, estimated using the SFD maps.

GRB 010222: Masetti et al. (2001) present a complete summary of the optical to NIR photometry (Lee et al. 2001, Cowsik et al. 2001, Jha et al. 2001, also see Frail et al. 2002, Mirabal et al. 2002a, Björnsson et al. 2002, Galama et al. 2003). A recent work from Frail et al. (2002) rules out that the K-band emission is originated from the burst or its afterglow and concludes that it is instead due to the emission of a high redshift starburst galaxy. We therefore excluded the K band point in our analysis. The galactic extinction in the direction of this burst is A_V=0.07, using the SFD maps.

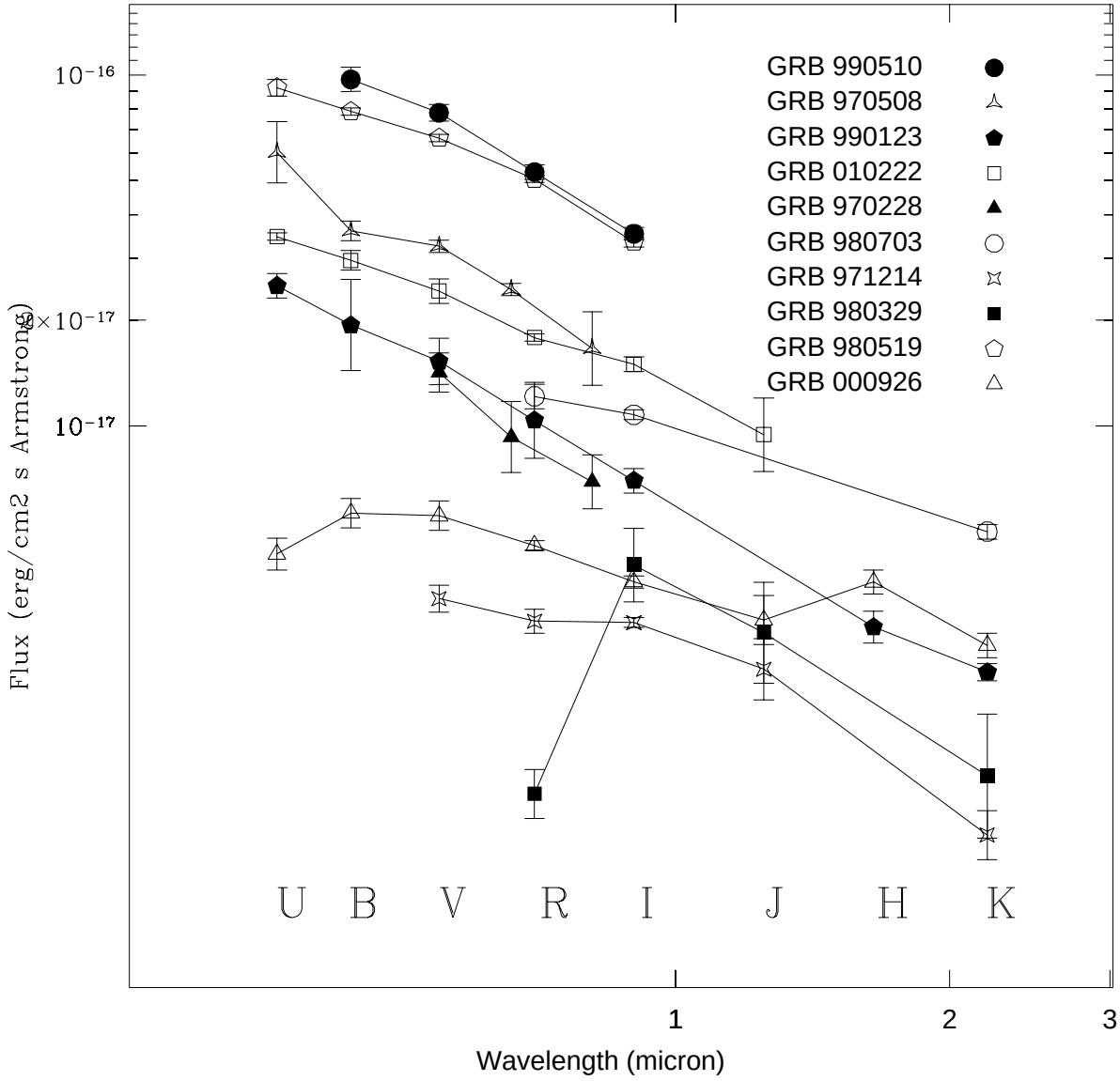

Fig. 1.— Spectral Energy Distribution for 9 of the 13 X-ray afterglows which have optical counterpart, plus GRB 000926 (see Appendix and Table 4)

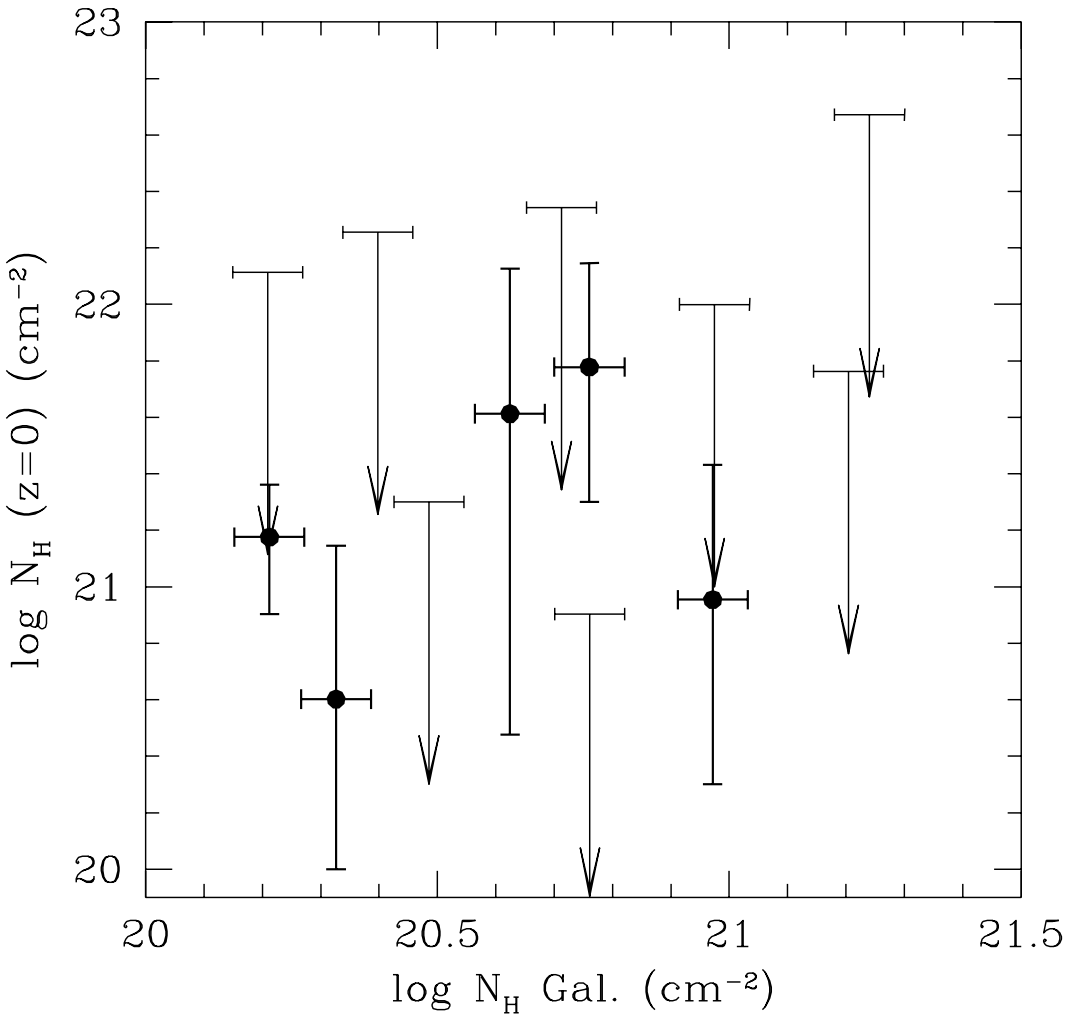

Fig. 2.— Best fit additional column density at z=0 against the Galactic column. Errors and upper limits (arrows) are at 90% confidence level for two parameters of interest ($\Delta\chi^2 = 4.61$). No trend is evident, supporting the robustness of our analysis (see §5.1).

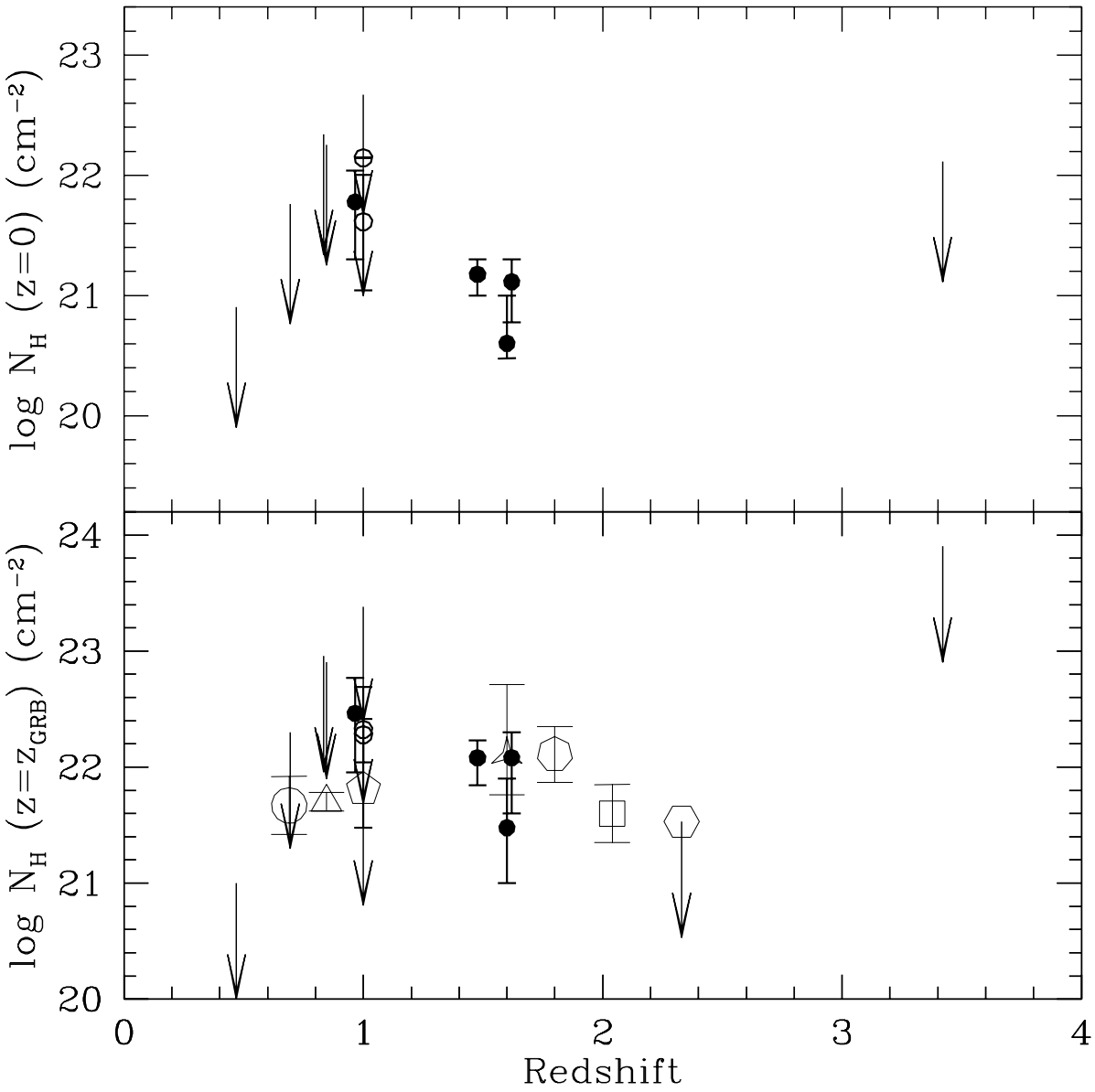

Fig. 3.— *Upper panel*: Additional column density at z=0 versus redshift. *Lower panel*: Additional column density at z=z_{GRB} (filled small circles) or z=1 for GRB with unknown redshift (open small circles) versus redshift. Errors and upper limits (arrows) are at 90% confidence level for two parameters of interest ($\Delta\chi^2 = 4.61$). In this panel are also shown the rest frame column densities estimated for GRB 000926 at z=2.04 (open square) and GRB 000210 at z=0.846 (open triangle) both from Piro et al. (2001,2002b), GRB 991216 at z=1.0 (open pentagon upper limit) from Ballantyne et al. (2002), GRB 020322 at z=1.8 (open eptagon) from Watson et al. (2002), GRB 020405 at z=0.690 (open circle) from Mirabal et al. (2002b), GRB 021004 at z=2.33 (open esagon upper limit) from Holland et al. (2002) and GRB 030227 at z$\sim$ 1.6 (open starred triangle) from Mereghetti et al. (2003) and from Watson et al. (2003).

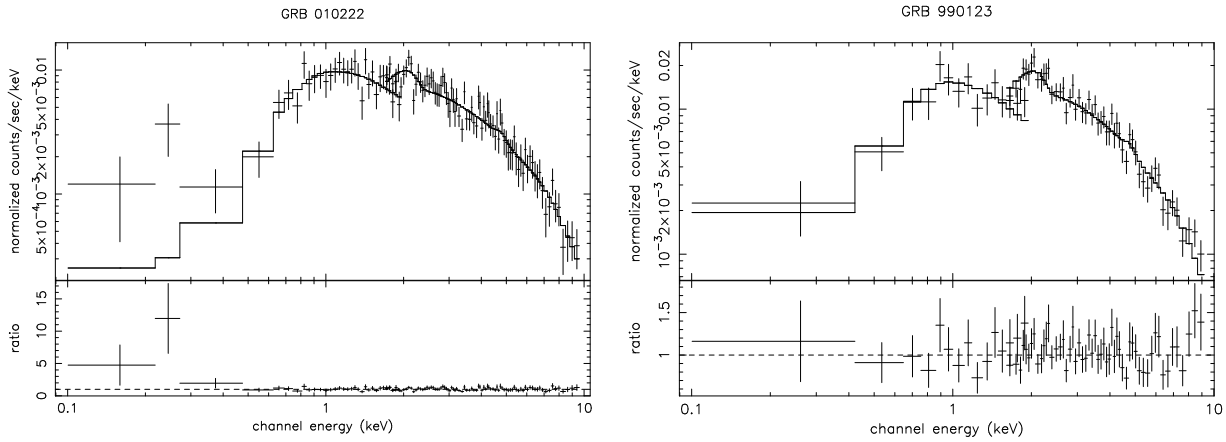

Fig. 4.— *Left:* LECS and MECS X-ray spectra of GRB 010222 *Right:* LECS and MECS X-ray spectra of GRB 990123. Both spectra are fitted by a simple power law and two neutral absorption components, one fixed to the Galactic value and the other free to vary at the redshift of the host galaxy. The residuals at low energies for GRB 010222 suggest the presence of complex absorption or an additive emission component.

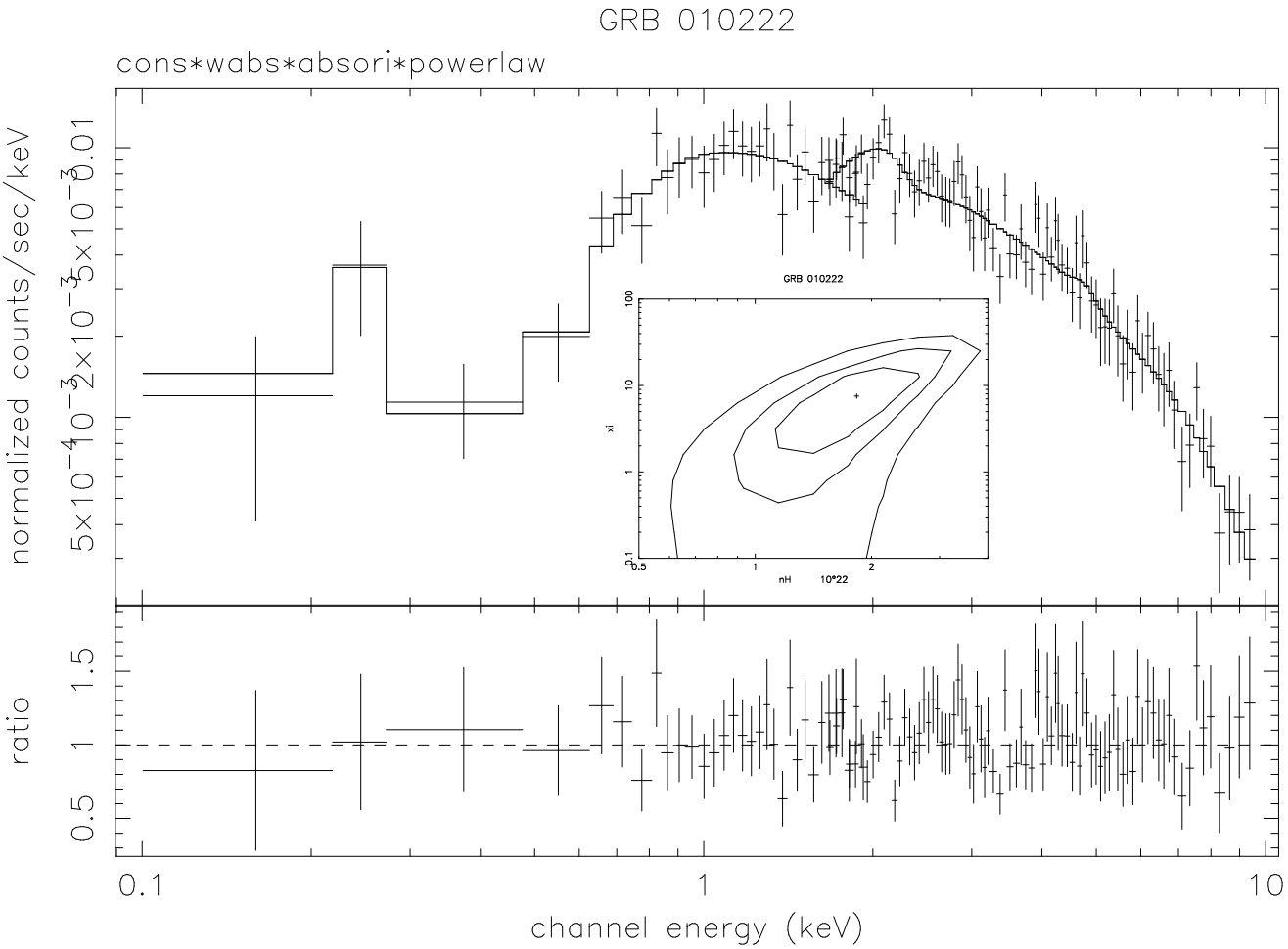

Fig. 5.— LECS and MECS X-ray spectra of GRB 010222 fitted with an ionized absorber ("absori" in XSPEC, see §5.1.1). The insert shows the χ^2 contours of the ionization parameter ξ and the rest frame column density N_H at 65%, 90% and 99% confidence levels.

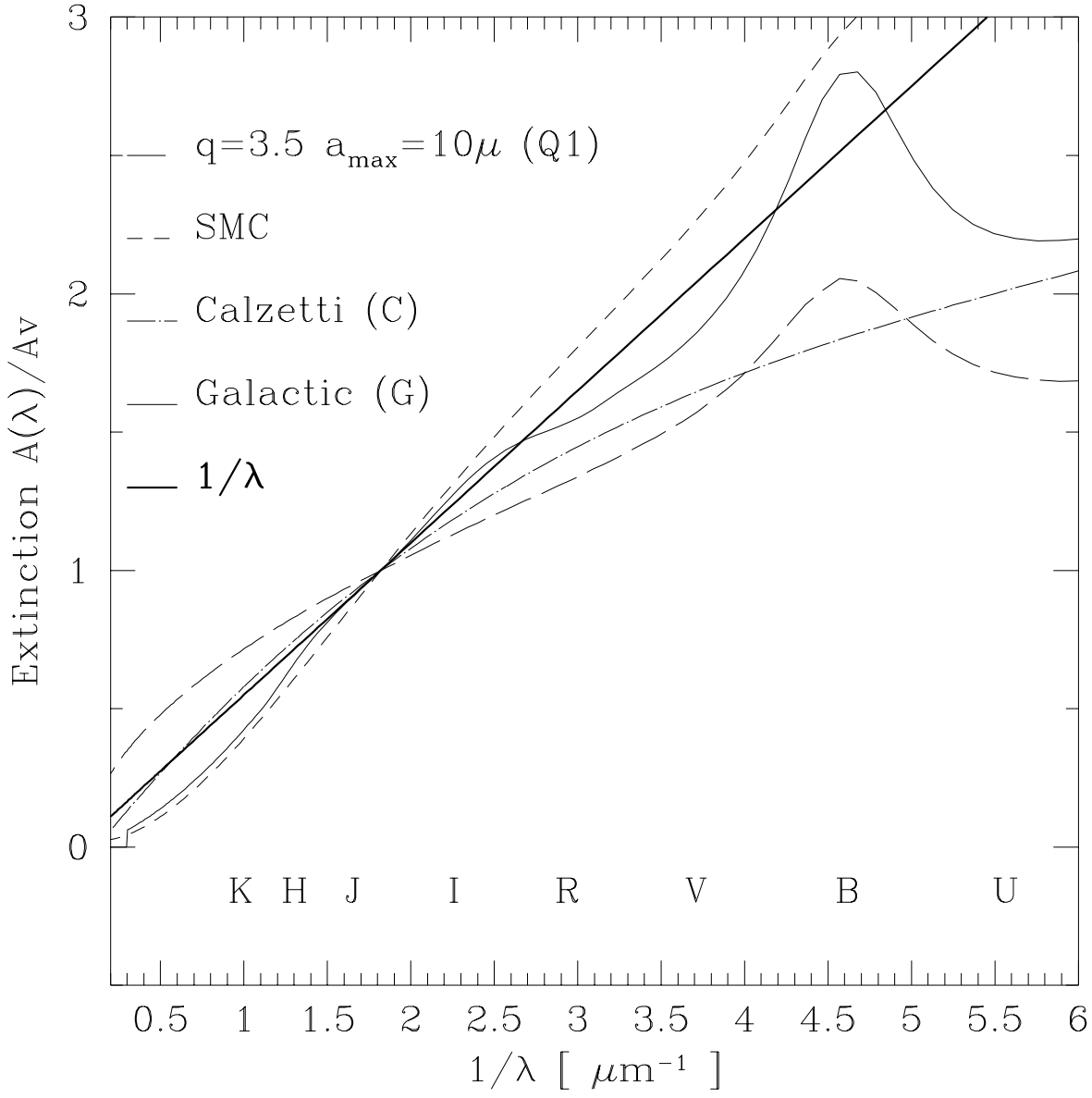

Fig. 6.— Extinction curves adopted in the analysis of the optical-NIR photometry against $1/\lambda$ (see §5.2). We indicate in the plot the rest frame wavelengths actually observed by a standard photometric system assuming z=1.

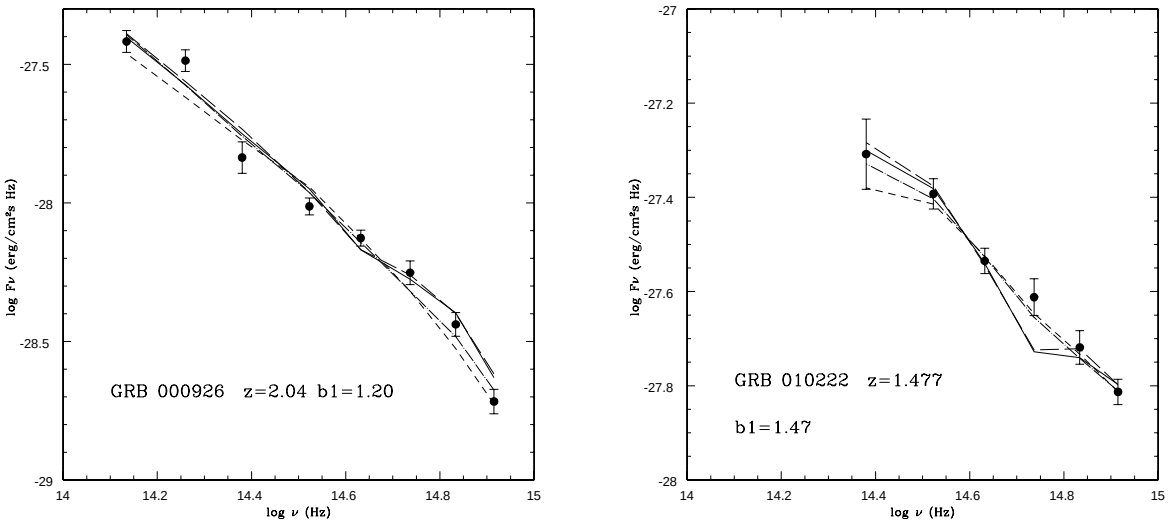

Fig. 7.— *Left:* The SED of GRB 000926 fitted with the four tested extinction models (line code is the same as in Figure 6). *Right:* The SED of GRB 010222 with the four tested extinction models. The 2175Å hump, typical of the extinction curves G and Q1, does not fit to GRB 010222. The C model (dot-dashed line) provides the minimum χ^2 among all the fitted models for both these bursts for $\nu_o < \nu_c$ (see §5.2.1 and Table 8).

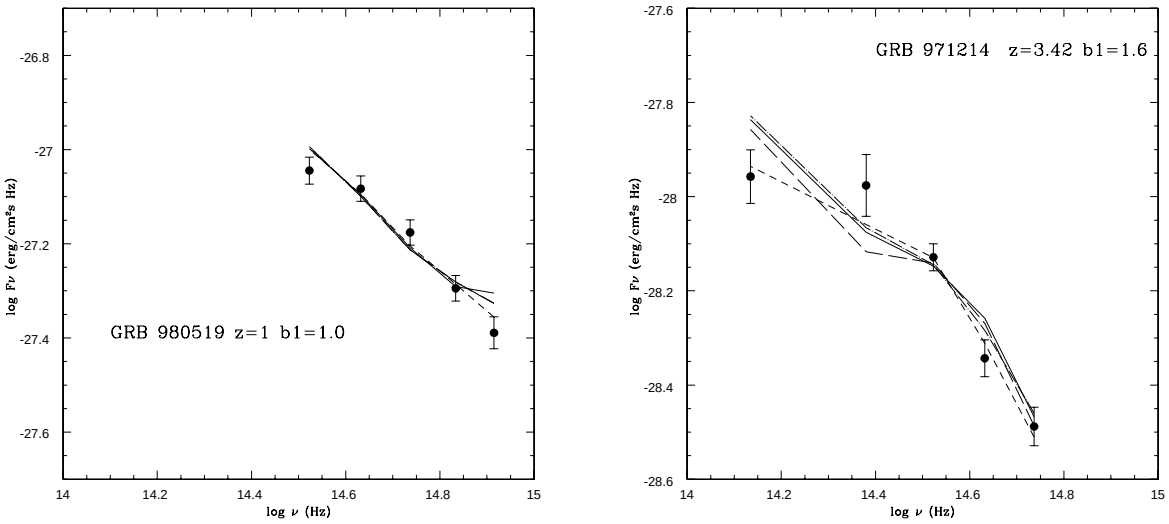

Fig. 8.— *Left*: The SED of GRB 980519 with the best fit models (line code is the same as in Figure 6). The SMC extinction curve (short dashed line) well fit to the data. In particular the extinction curves with the strong 2175 Å hump G and Q1, are not suitable to describe its SED at z=1. For lower redshift, the 2175 Å is shifted outside the photometric range of this burst. We found a minimum χ^2 for z=0.7 by using both the G and the Q1 extinction curves. *Right*: The SED of GRB 971214 with the best fit models (line code is the same as in Figure 6). The SMC extinction curve (short dashed line) provides the minimum χ^2 (see Tables 7 and 8).

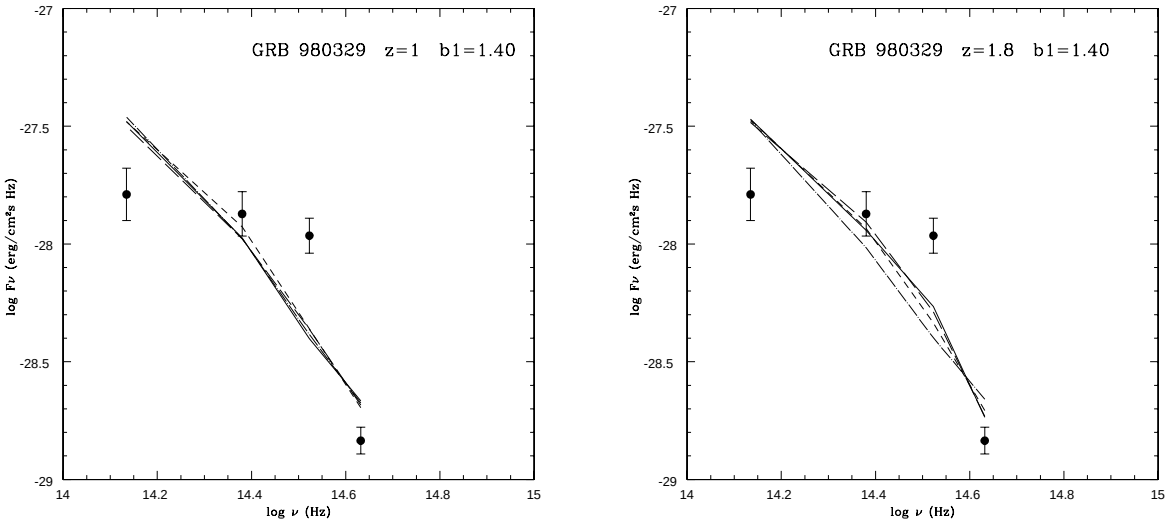

Fig. 9.— *Right.* The SED of GRB 980329 with the best fit models (line code is the same as in Figure 6) fixing the redshift z=1. *Left.* The SED of GRB 980329 with the best fit models obtained leaving the redshift free to vary. A minimum χ^2 is obtained at z=1.8 for all models. The jump between the R and I photometric points is marginally explained by the 2175 Å hump redshifted to the optical range (see §5.2.4). The same result is obtained for both the spectral index b_1 and b_2 (see Tables 7)

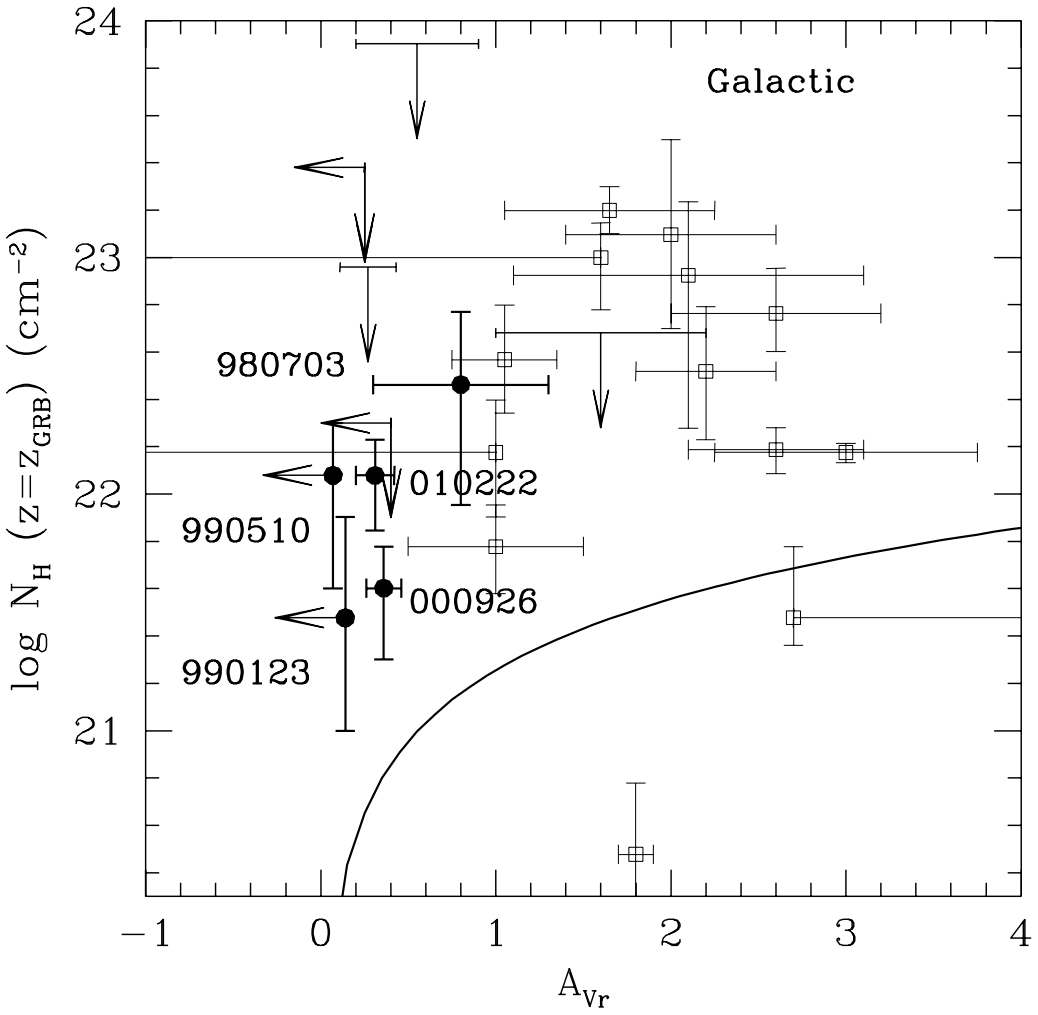

Fig. 10.— Best fit additional column densities (at the redshift of the GRB or at z=1 for the GRB with unknown redshifts) against best fit rest frame visual extinction A_{Vr} obtained assuming the Galactic (G) extinction curve (Cardelli et al. 1989). The A_{Vr} are estimated using the b_1 ($\nu_o < \nu_c$) optical afterglow power law indices (see Tables 7 and 8). Error bars are 68% confidence intervals. Upper limits are 90% confidence intervals. Small open squares are a sample of quasars from Maiolino et al. (2001b) and (Elvis et al. 1998). The solid line curve shows the expected values assuming a Galactic dust to gas mass ratio and the Galactic extinction model (Predehl & Smith 1995).

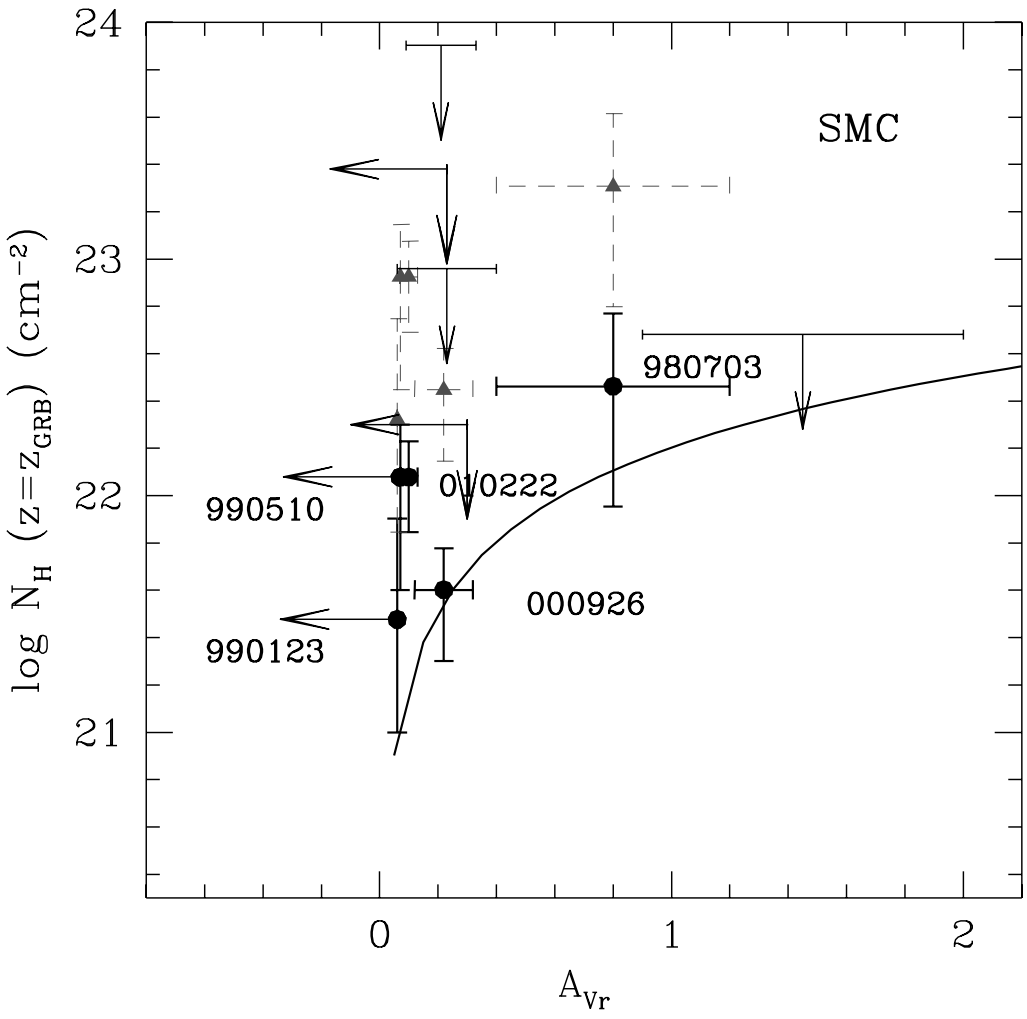

Fig. 11.— Best fit additional column densities against best fit visual extinction A_{Vr} (both at the redshift of the GRB or at z=1 for the GRB with unknown redshifts) obtained using the SMC extinction curve (Pei 1992). The A_{Vr} are estimated using the b_1 ($\nu_o < \nu_c$) optical afterglow power law indices (see Tables 7 and 8). Error bars are 68% confidence intervals and upper limits are 90% confidence intervals. The black dots with solid line error bars are the N_H measured assuming a solar metal abundance. The triangles with dashed line error bars are the N_H measured assuming a SMC environment which has a metal abundance ~ 8 times lower than the solar one. The solid line curve is the expected relationship between N_H and A_{Vr} for the SMC (Weingartner & Draine 2001).

.

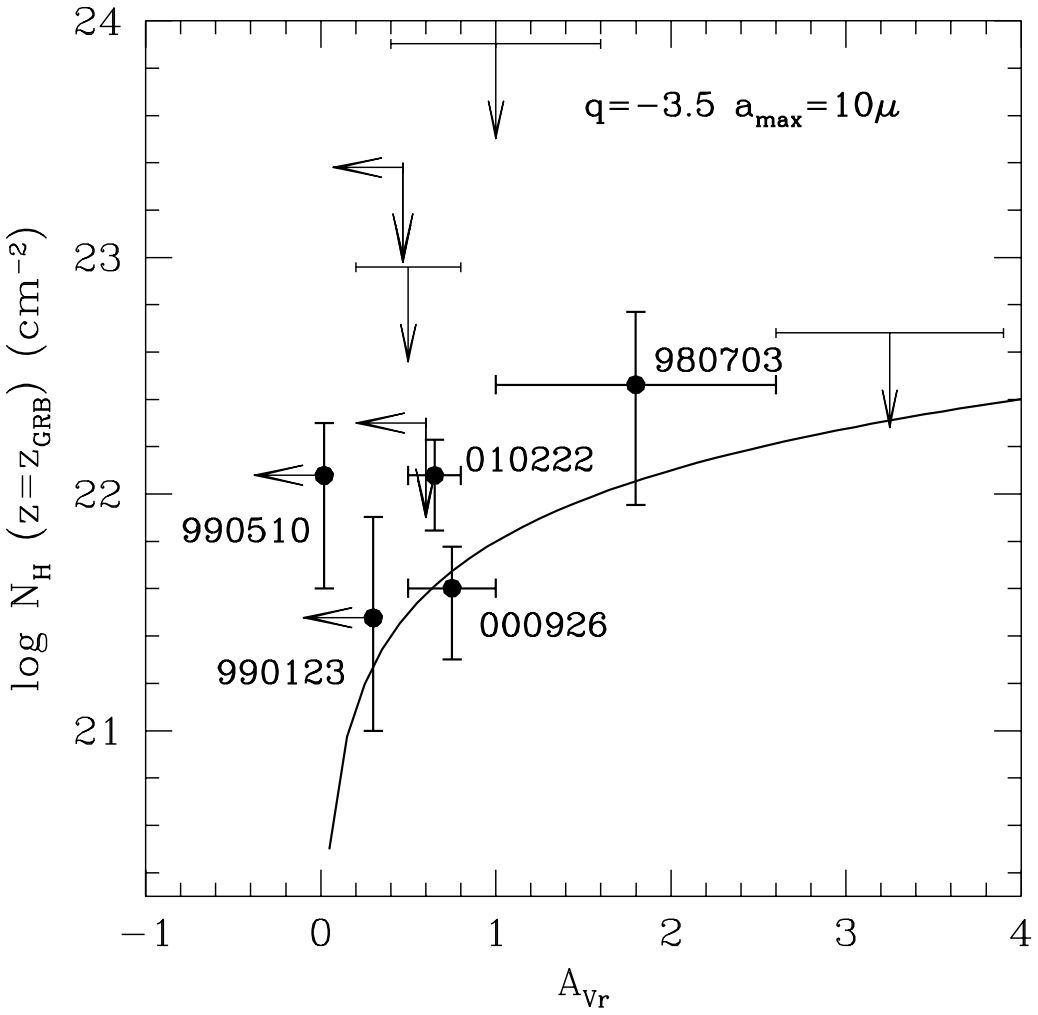

Fig. 12.— Best fit additional column densities against best fit visual extinction A_{Vr} (both at the redshift of the GRB or at z=1 for the GRB with unknown redshifts) obtained using the Maiolino et al. (2001a) extinction curve (Q1). The A_{Vr} are estimated using the b_1 ($\nu_o < \nu_c$) optical afterglow power law indices (see Tables 7 and 8). Error bars are 68% confidence intervals and upper limits are 90% confidence intervals. On the top-right of the plot are indicated the slope q of the dust grain size distribution and the maximum size a_{max} of the dust model used to derive the Q1 extinction curve. The solid line curve is the expected relationship between N_H and A_{Vr} for this models.

.

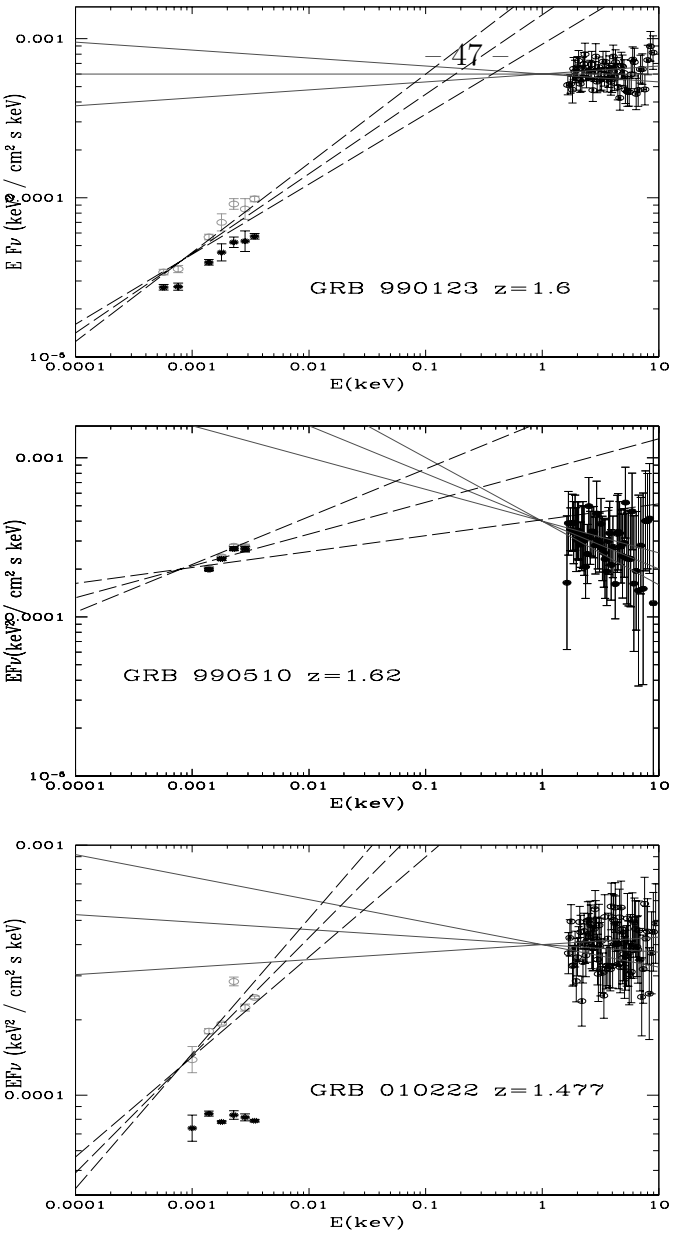

Fig. 13.— The EF_E NIR to X-ray SED of GRB 990123, GRB 990510 and GRB 010222. Optical fluxes have been corrected for both the Galactic and the extragalactic extinction. The latter was estimated using the best fit values obtained from the Q1 model for $\nu_o < \nu_c$. The normalization of the X-ray spectra has been scaled to the same time of the optical-NIR observations, using the published decay indices. The solid lines are the best fit X-ray power laws and their 90 % upper and lower limits, normalized at 1 keV. The dashed lines are NIR to UV power laws, computed from the X-ray spectral indices assuming the fireball models and normalized at 1 micron (observer frame).

Table 1: **The BeppoSAX bright afterglow sample.**

GRB	N_{HGal}[a] 10^{20} cm^{-2}	redshift	R.A.[b] h m s	Dec.[b] ° ′ ″	OT[c]
970228	16.0	0.6950 ± 0.0003[d]	15 28 0.9	+19 37 02	Y
970508	5.2	0.835 ± 0.001[e]	06 53 46.7	+79 16 02	Y
971214	1.6	3.418 ± 0.010[f]	11 56 25	+65 13 11	Y
980329	9.4	-	07 02 36	+38 50 24	Y
980519	1.7	-	23 22 22	+77 16 06	Y
980703	5.8	0.9661 ± 0.0001[g]	23 59 6.8	+08 35 45	Y
990123	2.1	1.600 ± 0.001[h]	15 25 30	+44 45 14	Y
990510	9.4	1.619 ± 0.002[i]	13 38 11.2	-80 30 02	Y
990704	3.1	-	12 19 27.3	-03 50 22	N
000210	2.5	0.8463 ± 0.0002[j]	01 59 09.8	-40 39 15	N
000214	5.8	0.47 ± 0.06[k]	18 54 27	-66 27 30	N
001109	4.2	-	18 30 07.8	+55 17 56	N
010222	1.6	1.4768 ± 0.0002[l]	14 52 12.0	+43 01 02	Y

[a] From Dickey & Lockman (1990). Uncertainties on these values are 16% at 1σ confidence level (see §3.1)

[b] From Narrow Field Instruments of BeppoSAX (J2000)

[c] Optical Transient

[d] Bloom et al. 2001

[e] Bloom et al. 1998b

[f] Kulkarni et al. 1998

[g] Djorgovski et al. 1998b

[h] Kulkarni et al. 1999

[i] Vreeswijk et al. 2000

[j] Piro et al. 2002b

[k] Antonelli et al. 2000 (from X-ray spectroscopy)

[l] Mirabal et al. 2002c

Table 2: **BeppoSAX LECS and MECS observations.**

	LECS 0.1-2.0keV				MECS 1.6-10.0keV			
GRB	Exposure[a]	r[b]	bkg[c]	source[d]	Exposure[a]	r[b]	bkg[c]	source[d]
	ks	arcmin	10^{-3}	10^{-3}	ks	arcmin	10^{-3}	10^{-3}
970228	5.5	$6'$	3.5 ± 0.1	18.2 ± 2.0	14.3	$3'$	1.5 ± 0.1	10.1 ± 0.9
970508	17.2	$6'$	3.8 ± 0.1	1.6 ± 0.8	28.2	$3'$	5.5 ± 0.1	6.6 ± 0.6
971214	45.5	$6'$	4.1 ± 0.1	1.5 ± 0.3	101.1	$3'$	3.5 ± 0.1	3.2 ± 0.3
980329	24.5	$3'$	1.2 ± 0.1	0.9 ± 0.3	63.8	$3'$	3.5 ± 0.1	3.3 ± 0.3
980519	22.7	$4'$	2.1 ± 0.1	0.3 ± 0.6	77.8	$3'$	3.5 ± 0.1	6.0 ± 0.8
980703	16.3	$4'$	2.0 ± 0.1	1.4 ± 0.5	39.1	$4'$	3.4 ± 0.1	5.9 ± 0.5
990123	15.1	$4'$	2.1 ± 0.1	18.4 ± 1.2	45.2	$3'$	3.5 ± 0.1	42.9 ± 1.0
990510	31.2	$4'$	2.0 ± 0.1	7.1 ± 0.6	67.9	$3'$	3.5 ± 0.1	16.8 ± 0.5
990704	13.4	$4'$	2.1 ± 0.1	4.3 ± 1.4	37.0	$3'$	3.5 ± 0.1	5.8 ± 0.5
000210	15.7	$6'$	4.6 ± 0.1	2.6 ± 0.8	44.4	$3'$	3.5 ± 0.1	3.1 ± 0.4
000214	14.8	$4'$	2.1 ± 0.1	1.5 ± 0.5	50.8	$3'$	3.5 ± 0.1	3.8 ± 0.4
001109	19.2	$4'$	2.1 ± 0.1	1.2 ± 0.4	85.4	$3'$	3.6 ± 0.1	3.2 ± 0.3
010222	50.3	$4'$	2.1 ± 0.1	11.7 ± 0.5	88.4	$3'$	3.5 ± 0.1	24.3 ± 0.6

[a]Net exposure time

[b]Radius of source extraction region (see §3)

[c]Background count rates

[d]Net source count rates

Table 3: **BeppoSAX NFI observations.**

GRB	MECS off-axis[a] arcmin	$(T_{start} - T_{GRB})^b$ h	$(T_{end} - T_{GRB})^b$ h	LECS RAW Coord.[c] Pixels
970228	0.4	8.0	17.0	118.4,155.0
970508	0.4	5.7	15.7	112.9,116.6
971214	1.9	6.7	60.8	132.6,123.5
980329	1.6	7.0	48.5	134.2,126.9
980519	1.7	9.7	34.2	135.6,135.8
980703	1.7	22.3	45.8	132.1,119.8
990123	1.7	5.8	32.2	130.1,125.3
990510	1.6	8.0	52.3	139.2,128.5
990704	1.6	8.0	29.9	134.1,119.4
000210	1.6	7.2	38.9	131.8,133.7
000214	1.7	12.0	40.9	138.0,119.2
001109	1.7	16.5	38.3	129.4,124.1
010222	0.8	8.0	65.0	128.0,131.9

[a] off-axis angle on the MECS detector

[b] elapsed time of NFI first TOO from the time of the GRB detection

[c] 'raw' detector pixel coordinates of the source at which the effective area has been computed.

Table 4: **The optical-near infrared magnitudes of the bright afterglow sample.**

GRB(UT)	U	B	V	R	I	J	H	K
970228.12[1]	-	-	21.01 ± 0.16	20.91 ± 0.29^{Rc}	20.51 ± 0.22^{Ic}	-	-	-
970508.90[2]	19.63 ± 0.25	20.59 ± 0.08	20.11 ± 0.05	19.86 ± 0.05^{Rc}	19.56 ± 0.30^{Ic}	-	-	-
971214.97[3]	-	-	22.62 ± 0.11	22.07 ± 0.10	21.30 ± 0.04	20.45 ± 0.25	-	19.45 ± 0.2
980329.15[4]	-	-	-	23.30 ± 0.20	20.89 ± 0.30	20.19 ± 0.41	-	19.03 ± 0.5
980519.51[5]	19.17 ± 0.07	19.74 ± 0.03	19.34 ± 0.03	18.92 ± 0.03	18.59 ± 0.04	-	-	-
980703.18[6]	-	-	-	21.18 ± 0.07	20.54 ± 0.61	-	-	17.55 ± 0.47
990123.41[7]	20.58 ± 0.10	21.26 ± 0.37	20.93 ± 0.19	20.64 ± 0.31	20.29 ± 0.10	-	19.12 ± 0.13	18.29 ± 0.07
990510.37[8]	-	19.51 ± 0.11	19.16 ± 0.09	18.87 ± 0.08	18.53 ± 0.07	-	-	-
000926.99[10]	22.49 ± 0.13	22.6 ± 0.12	22.03 ± 0.12	21.53 ± 0.04	21.01 ± 0.05	20.1 ± 0.2	18.8 ± 0.1	18.1 ± 0.1
010222.31[9]	20.23 ± 0.03	20.80 ± 0.08	20.43 ± 0.10	20.05 ± 0.01	19.46 ± 0.06	18.78 ± 0.3	host gal?	host gal?

[1] From Galama et al. (2000), t_0=UT 28.99 (t_0=extrapolation time, see §4. In this case this is at +20.9h from the gamma-ray event); [2]Galama et al. (1998a), t_0=UT 10.98 (+49.8h); [3]Ramaprakash et al. (1998), t_0=UT 15.51 (+12.9h); [4]Reichart et al. (1999b), t_0=UT 29.99 (+19.9h); [5]Jaunsen et al. (2001), t_0=UT 19.96 (+10.7h); [6]Vreeswijk et al. (1999), t_0=UT 4.4 (+29.2h); [7]Galama et al. (1999), t_0=UT 24.65 (+29.8h); [8]Stanek et al. (1999), t_0=UT 11.26 (+21.4h); [9]Masetti et al. (2001), t_0= UT 23.28 (+23.4h); [10]Fynbo et al. (2001), t_0=UT 29.67 (+64.3h).

Table 5: **BeppoSAX LECS and MECS spectral fits in the 0.1-10.0 keV band.**

GRB	LECS-MECS[a] constant	N_H[b] 10^{22} cm^{-2}	z	α_X[c]	χ^2(dof)	P(F)[d] %
971214	0.7-1.4	$80^{u.l.}$	3.42	$0.9^{+1.0}_{-0.6}$	34.12 (42)	93.3
		0 fixed	3.42	0.56 ± 0.26	36.99 (43)	
		$1.3^{u.l.}$	0	$0.8^{+0.6}_{-0.4}$	34.79 (42)	
990123	0.57-0.69	$0.3^{+0.7}_{-0.2}$	1.60	1.0 ± 0.1	55.94 (66)	> 99.99
		0 fixed	1.60	$0.9^{+0.08}_{-0.05}$	70.44 (67)	
		$0.04^{+0.07}_{-0.03}$	0	1.0 ± 0.1	55.73 (66)	
990704	0.6-1.0	$9^{u.l.}$	1	$1.2^{+0.8}_{-0.5}$	17.36 (16)	92.5
		0 fixed	1	0.7 ± 0.3	21.29 (17)	
		$1.4^{u.l.}$	0	$1.0^{+0.3}_{-0.2}$	17.24 (16)	
000210	0.9-2.2	$8.0^{u.l.}$	0.846	$1.5^{+0.9}_{-0.7}$	12.63 (13)	89.9
		0 fixed	0.846	$1.1^{+0.5}_{-0.6}$	15.65 (14)	
		$1.8^{u.l.}$	0	$1.5^{+1.4}_{-0.7}$	12.77 (13)	
001109	0.4-1.2	$1.9^{+4.7}_{-1.8}$	1	1.4 ± 0.6	29.09 (27)	97.0
		0 fixed	1	$1.1^{+0.3}_{-0.4}$	34.70 (28)	
		$0.4^{+0.9}_{-0.4}$	0	$1.4^{+0.7}_{-0.6}$	29.10 (27)	
010222	1.21-1.37	$1.2^{+0.7}_{-0.6}$	1.477	1.0 ± 0.1	99.80 (111)	> 99.99
		0 fixed	1.477	$0.82^{+0.04}_{-0.08}$	146.11 (112)	
		$0.15^{+0.08}_{-0.07}$	0	1.0 ± 0.1	104.61 (111)	

u.l. = *upper limit* at 90% confidence level for two parameters of interest ($\Delta\chi^2 = 4.61$).

[a]ECS-MECS normalization constant interval at 68% confidence level

[b]Equivalent hydrogen column density. Errors at 90% confidence level for two parameters of interest ($\Delta\chi^2 = 4.61$).

[c]Power law spectral index. Error at 90% confidence level for two parameters of interest ($\Delta\chi^2 = 4.61$).

[d]P(F) is the confidence level for the inclusion of additional column density, computed using the F test (Bevington & Robinson 1992).

Table 6: **BeppoSAX LECS and MECS spectral fits in the 0.4-10 keV band.**

GRB	MECS-LECS constant	N_H 10^{22} cm^{-2}	z (fixed)	α_X	χ^2(dof)	P(F) %
970228	0.6-1.0	$2^{u.l.}$	0.695	1.1 ± 0.5	6.90 (10)	90.8
		0 fixed	0.695	$0.8^{+0.3}_{-0.1}$	9.29 (11)	
		$0.58^{u.l.}$	0	1.1 ± 0.5	7.00 (10)	
970508	0.4-1.0	$9.1^{u.l.}$	0.835	$0.8^{+0.4}_{-0.3}$	7.38 (12)	90.7
		0 fixed	0.835	0.5 ± 0.3	9.43 (13)	
		$2.2^{u.l.}$	0	$0.8^{+0.6}_{-0.4}$	7.43 (12)	
980329	0.6-0.9	$4.8^{u.l.}$	1	$1.1^{+0.7}_{-0.5}$	15.75 (17)	-
		0 fixed	1	$1.1^{+0.5}_{-0.4}$	15.80 (18)	
		$1.0^{u.l.}$	0	$1.2^{+0.6}_{-0.5}$	15.70 (17)	
980519	0.7-0.9	$24^{u.l.}$	1	$1.5^{+1.6}_{-1.0}$	15.95 (8)	50.3
		0 fixed	1	$1.1^{+0.6}_{-0.5}$	16.96 (9)	
		$4.7^{u.l.}$	0	$1.6^{+1.9}_{-1.1}$	15.91 (8)	
980703	0.4-1.0	$2.9^{+7.1}_{-2.7}$	0.966	$1.8^{+0.8}_{-0.5}$	23.30 (20)	97.5
		0 fixed	0.966	1.3 ± 0.3	30.12 (21)	
		$0.6^{+0.8}_{-0.4}$	0	$1.7^{+1.3}_{-0.5}$	24.45 (20)	
990510	0.6-0.8	$1.6^{+1.9}_{-1.3}$	1.62	1.3 ± 0.2	75.13 (65)	98.3
		0 fixed	1.62	$1.16^{+0.08}_{-0.11}$	83.11 (66)	
		$0.16^{+0.24}_{-0.14}$	0	1.3 ± 0.2	76.43 (65)	
000214	0.3-0.7	$0.1^{u.l.}$	0.47	2.0 ± 0.6	42.03 (20)	-
		0 fixed	0.47	2.0 ± 0.6	41.96(21)	
		$0.08^{u.l.}$	0	2.0 ± 0.6	42.03(20)	

Table 7: **Optical afterglow spectral fits.**

GRB	Models	$\nu_o < \nu_c$			$\nu_o > \nu_c$		
		b_1	A_{Vr}	$\chi^2/d.o.f.$	b_2	A_{Vr}	$\chi^2/d.o.f.$
970228	G	1.4 ± 0.3	< 0.4	0.95/1	0.9 ± 0.3	< 0.2	2.7/1
z=0.695	SMC	1.4 ± 0.3	< 0.3	0.95/1	0.9 ± 0.3	< 0.1	2.7/1
$p = 2.2 \pm 0.6$	Q1	1.4 ± 0.3	< 0.6	0.96/1	0.9 ± 0.3	< 0.3	2.7/1
	C	1.4 ± 0.3	< 0.7	0.90/1	0.9 ± 0.3	< 0.4	2.7/1
970508	G	1.7 ± 0.2	0.27 ± 0.16	1.9/3	1.2 ± 0.2	< 0.23	4.3/3
z=0.835	SMC	1.7 ± 0.2	0.23 ± 0.17	4.1/3	1.2 ± 0.2	< 0.19	5.0/3
$p = 1.6 \pm 0.4$	Q1	1.7 ± 0.2	0.5 ± 0.3	2.2/3	1.2 ± 0.2	< 0.4	4.4/3
	C	1.7 ± 0.2	0.8 ± 0.6	4.8/3	1.2 ± 0.2	< 0.7	7.5/3
971214	G	1.6 ± 0.5	0.55 ± 0.35	4.3/1	1.1 ± 0.5	< 0.6	2.5/1
z=3.42	SMC	1.6 ± 0.5	0.21 ± 0.12	0.7/1	1.1 ± 0.5	< 0.24	0.6/1
$p = 1.8 \pm 1.0$	Q1	1.6 ± 0.5	1.0 ± 0.6	2.9/1	1.1 ± 0.5	< 1.2	1.8/1
	C	1.6 ± 0.5	1.35 ± 0.85	1.1/1	1.1 ± 0.5	< 1.7	0.8/1
971214(*)	G	1.6 ± 0.5	< 0.46	10.2/3	1.1 ± 0.5	< 0.5	14.1/3
	SMC	1.6 ± 0.5	0.2 ± 0.1	5.0/3	1.1 ± 0.5	< 0.22	11.0/3
	Q1	1.6 ± 0.5	0.76 ± 0.74	8.9/3	1.1 ± 0.5	< 0.1	13.3/3
	C	1.6 ± 0.5	0.85 ± 0.84	8.8/3	1.1 ± 0.5	< 1.1	13.7/3
980329	G	1.40 ± 0.35	1.6 ± 0.6	20.8/2	0.90 ± 0.35	1.2 ± 0.6	21.2/2
z=1	SMC	1.40 ± 0.35	1.45 ± 0.55	17.2/2	0.90 ± 0.35	1.1 ± 0.6	18.4/2
$p = 2.2 \pm 0.7$	Q1	1.40 ± 0.35	3.25 ± 0.65	17.8/2	0.90 ± 0.35	2.5 ± 1.2	18.9/2
	C	1.40 ± 0.35	3.2 ± 0.7	19.7/2	0.90 ± 0.35	2.35 ± 1.15	20.4/2
980519	G	1.0 ± 0.8	< 0.25	29.3/3	0.5 ± 0.8	< 0.03	27.3/3
z=1	SMC	1.0 ± 0.8	< 0.23	16.3/3	0.5 ± 0.8	< 0.02	26.7/3
$p = 3.0 \pm 1.6$	Q1	1.0 ± 0.8	< 0.47	38.0/3	0.5 ± 0.8	< 0.05	27.6/3
	C	1.0 ± 0.8	< 0.84	28.1/3	0.5 ± 0.8	< 0.02	27.6/3
980703	G	0.7 ± 0.4	0.8 ± 0.5	3.6/1	0.2 ± 0.4	0.5 ± 0.5	3.7/1
z=0.966	SMC	0.7 ± 0.4	0.8 ± 0.4	7.2/1	0.2 ± 0.4	0.4 ± 0.3	5.4/1
$p = 3.6 \pm 0.8$	Q1	0.7 ± 0.4	1.8 ± 0.8	7.4/1	0.2 ± 0.4	0.9 ± 0.8	5.5/1
	C	0.7 ± 0.4	1.7 ± 0.7	5.0/1	0.2 ± 0.4	0.9 ± 0.8	4.4/1

Note. — In the first column there are the burst name, the redshift and the electron spectral index value p derived from the X-ray spectral index (Tab. 5-6) assuming that $\nu_X > \nu_c$. For GRB 000926 see §5.2. In the second column, there are the extinction models: G=Galactic, SMC=Small Magellanic Clouds, Q1 is from dust model with large grain (q=3.5, $a_{max} = 10\mu$), C=starburst galaxies extinction curve from Calzetti (1994). The b_1 and b_2 optical afterglow power law index are obtained from the electron spectral index value p according to the standard fireball model for the case $\nu_o < \nu_c$ and $\nu_o > \nu_c$ (see §5.2). Errors and upper limits are at 68% confidence level.

(*)We are here fitting also the J and K bands (see Appendix).

Table 8: **Continue.**

GRB	Models	$\nu_o < \nu_c$			$\nu_o > \nu_c$		
		b_1	A_{Vr}	χ^2	b_2	A_{Vr}	χ^2
990123	G	1.50 ± 0.06	< 0.14	2.9/5	1.00 ± 0.06	< 0.03	45.2/5
z=1.60	SMC	1.50 ± 0.06	< 0.06	3.1/5	1.00 ± 0.06	< 0.02	45.2/5
$p = 2.0 \pm 0.1$	Q1	1.50 ± 0.06	< 0.3	2.9/5	1.00 ± 0.06	< 0.01	45.2/5
	C	1.50 ± 0.06	< 0.3	2.6/5	1.00 ± 0.06	< 0.01	45.2/5
990510	G	1.20 ± 0.10	< 0.07	22.6/2	0.7 ± 0.1	< 0.04	62.9/2
z=1.62	SMC	1.20 ± 0.10	< 0.07	22.6/2	0.7 ± 0.1	< 0.01	64.1/2
$p = 2.6 \pm 0.2$	Q1	1.20 ± 0.10	< 0.02	22.6/2	0.7 ± 0.1	< 0.01	62.9/2
	C	1.20 ± 0.10	< 0.01	22.6/2	0.7 ± 0.1	< 0.01	62.9/2
000926	G	1.20 ± 0.15	0.36 ± 0.10	26.9/6	0.70 ± 0.15	0.15 ± 0.11	22.6/6
z=2.04	SMC	1.20 ± 0.15	0.22 ± 0.10	30.4/6	0.70 ± 0.15	0.10 ± 0.07	22.4/6
$p = 2.6 \pm 0.3$	Q1	1.20 ± 0.15	0.75 ± 0.25	23.1/6	0.70 ± 0.15	0.34 ± 0.25	21.1/6
	C	1.20 ± 0.15	1.34 ± 0.29	16.7/6	0.70 ± 0.15	0.41 ± 0.30	19.6/6
010222	G	1.47 ± 0.07	0.31 ± 0.11	11.2/4	0.97 ± 0.07	< 0.02	7.7/4
z=1.477	SMC	1.47 ± 0.07	0.10 ± 0.03	2.9/4	0.97 ± 0.07	< 0.1	7.6/4
$p = 2.06 \pm 0.14$	Q1	1.47 ± 0.07	0.65 ± 0.15	10.8/4	0.97 ± 0.07	< 0.06	7.7/4
	C	1.47 ± 0.07	0.56 ± 0.18	2.4/4	0.97 ± 0.07	< 0.04	7.7/4